

HIGH TEMPERATURE OXIDATION AND SURFACE MODIFICATION OF
BINARY ALUMINIDE INTERMETALLIC COMPOUNDS USING ION
IMPLANTATION OF OXYGEN

By
ROBERT JOSEPH HANRAHAN JR.

A DISSERTATION PRESENTED TO THE GRADUATE SCHOOL OF THE
UNIVERSITY OF FLORIDA IN PARTIAL FULFILLMENT OF THE
REQUIREMENTS FOR THE DEGREE OF DOCTOR OF PHILOSOPHY

UNIVERSITY OF FLORIDA

1994

Copyright 1994

By

Robert Joseph Hanrahan Jr.

ACKNOWLEDGMENTS

In the 13 years during which I have studied at the University of Florida, so many people have assisted me that it is impossible to list them all. I will attempt to mention a few the individuals without whom this work would never have pursued. First I would like to thank Dr. Ellis D Verink Jr. who served as chairman of my committee and as the inspiration for me enter the field of metallurgy.

Both the Materials Science and the Nuclear Engineering Departments of the College of Engineering have been generous in their stimulating educational and financial support. In addition to the faculty members I have worked with, I would like to thank the secretaries in both of these departments without whom I often might have despaired of completing the endless paperwork required of a professional student.

The support for the portion of this research which was performed at Oak Ridge National Laboratory was sponsored by the Division of Materials Science, U.S. Department of Energy, under contract DE-AC05-84OR21400 with Martin Marietta Energy Systems Inc. I especially want to than Dr. Stephen P. Withrow of ORNL for his direct assistance with all of the implantation work.

All of the technicians at MAIC have been very helpful to me. I particularly want to single out Eric Lambers for his assistance with surface analysis. Dr. M. P. Lambers at

Microfabritech was patient and helpful beyond the call of duty in performing most of the SIMS analysis used in this work.

The assistance of Dr. Darryl Butt at Los Alamos National Laboratory, particularly in providing me with a quiet place to work while I wrote the bulk of this dissertation, is gratefully acknowledged.

Finally I would like to thank my family, and especially my father, Dr. Robert Hanrahan, without whose patient support I never would have completed any of the milestones in my life or my academic career.

TABLE OF CONTENTS

| | |
|---|-----|
| ACKNOWLEDGEMENTS | iii |
| ABSTRACT | vii |
| CHAPTER 1 INTRODUCTION | 1 |
| CHAPTER 2 REVIEW OF LITERATURE | 4 |
| Oxidation of NbAl ₃ , TiAl, and NiAl | 4 |
| Oxidation of NbAl ₃ | 4 |
| Oxidation of TiAl | 6 |
| Oxidation of NiAl | 8 |
| Summary of Oxidation Studies | 11 |
| Effects of Ion Implantation on Pure Metals and Alloys | 12 |
| Pure Metals | 12 |
| Implantation of Alloys and Oxides | 16 |
| Summary of Ion Implantation Literature Review | 23 |
| CHAPTER 3 EXPERIMENTAL TECHNIQUES | 25 |
| Materials Preparation | 25 |
| Ion Implantation | 26 |
| Test Environments | 27 |
| Analytical Techniques | 28 |
| Auger Electron Spectroscopy | 29 |
| Secondary Ion Mass Spectrometry | 29 |
| X-Ray Diffraction | 31 |
| Microscopy | 32 |
| X-Ray Photoelectron Spectroscopy | 32 |
| CHAPTER 4 OXYGEN IMPLANTED NbAl ₃ | 34 |
| Ion Implantation | 34 |
| Oxidation and Annealing Treatments | 41 |
| Surface Analysis | 42 |
| Secondary Ion Mass Spectrometry | 51 |
| Introduction | 51 |
| As-Implanted NbAl ₃ | 55 |
| Annealed NbAl ₃ | 56 |
| Oxidized NbAl ₃ | 62 |
| Influence of Ion Implanted Oxygen on the mechanism of Pest in NbAl ₃ | 71 |
| X-ray Diffraction | 78 |
| Summary Of Results of Implantation of Oxygen In NbAl ₃ | 79 |
| CHAPTER 5 OXYGEN IMPLANTED TiAl | 81 |

| | |
|--|-----|
| Ion Implantation ----- | 81 |
| Surface Analysis - Auger Electron Spectroscopy ----- | 83 |
| Secondary Ion Mass Spectrometry ----- | 93 |
| Introduction ----- | 93 |
| As-Implanted TiAl ----- | 93 |
| Annealed Oxygen-Implanted TiAl ----- | 96 |
| Oxidized Oxygen-Implanted TiAl ----- | 99 |
| CHAPTER 6 OXYGEN IMPLANTED NiAl ----- | 110 |
| Ion Implantation ----- | 110 |
| Auger Electron Spectroscopy ----- | 113 |
| X-Ray Diffraction ----- | 118 |
| Secondary Ion Mass Spectrometry ----- | 122 |
| Introduction ----- | 122 |
| As-Implanted NiAl ----- | 123 |
| Annealed Oxygen-Implanted NiAl ----- | 126 |
| Oxidized Oxygen-Implanted NiAl ----- | 139 |
| Cyclic Oxidation of Oxygen-Implanted NiAl ----- | 140 |
| Summary ----- | 143 |
| CHAPTER 7 SUMMARY AND CONCLUSIONS ----- | 147 |
| Review of Research Objectives ----- | 147 |
| Oxygen Implanted NbAl ₃ ----- | 147 |
| Oxygen Implanted TiAl ----- | 149 |
| Oxygen Implanted NiAl ----- | 150 |
| REFERENCES ----- | 152 |
| BIOGRAPHICAL SKETCH ----- | 158 |

Abstract of Dissertation Presented to the Graduate School of the University of Florida in
Partial Fulfillment of the Requirements for the Degree of Doctor of Philosophy

HIGH TEMPERATURE OXIDATION AND SURFACE MODIFICATION OF
BINARY ALUMINIDE INTERMETALLIC COMPOUNDS USING ION
IMPLANTATION OF OXYGEN

By

Robert Joseph Hanrahan Jr.

December 1994

Chairman: Ellis D. Verink Jr.

Major Department: Materials Science and Engineering

This work presents a novel approach to the modification of intermetallic compounds to achieve improved oxidation resistance. In order to bypass problems associated with the transient oxidation stage of alloys and intermetallic compounds, high-dose implants of oxygen are used to form a continuous oxygen saturated layer at room temperature. In order to study the implanted layer using secondary ion mass spectrometry ^{18}O is used as the implanted species. Three different aluminides have been investigated.

With NbAl_3 it was found that oxidation at 1000°C resulted in significantly thinner protective alumina scales on the oxygen implanted surfaces. Exposure at 760°C to an atmosphere containing 50 ppm oxygen was used to induce pest. The oxygen implanted surfaces showed significantly improved resistance to pesting. The implanted surfaces were

found to have much less oxygen penetration below the surface than the non-implanted surfaces. An interpretation of the controlling mechanism of pest is presented.

In TiAl the as-implanted material was found to form a layer containing primarily aluminum oxide. After brief exposures at 1000° C the implanted surfaces were found to form titanium oxide scales which were thicker than those formed on the non-implanted surfaces. Using specimens implanted with ²⁰Ne this phenomenon was shown to be due to the effect of damage to the surface.

In NiAl a well defined oxide layer was formed by the implanted oxygen after annealing at 1000° C. This layer was shown to be completely stable after exposures of up to 1 hour. The oxide layer appears to recrystallize as NiAl₂O₄ with an epitaxial relationship to the substrate. The implanted oxide layer was shown to result in significantly improved oxidation resistance under both isothermal and cyclic exposure at 1000° C.

This research proves the principal that oxygen implantation can be used as a technique for forming in-situ coatings on aluminide intermetallic compounds that in some cases result in significantly improved oxidation resistance by modifying the initial oxidation kinetics of the material.

CHAPTER 1 INTRODUCTION

Driven by the needs of the aerospace industry for a "next generation material," research into the properties of intermetallic compounds, particularly aluminides and silicides, has been ongoing (albeit unevenly) since the introduction of superalloys. However in spite of over thirty years of research no monolithic intermetallic compound has been used as a structural material in a production aircraft. Oxidation of intermetallics is one of the key obstacles to the use of this class of materials.

Much of the work on intermetallics for high temperature applications has focused on aluminide compounds which contain enough Al that they might oxidize to form a protective alumina scale. In practice however, the protectiveness of the scale can be compromised by numerous processes: formation of nonprotective, fast growing, "transient" oxides, transformation to phases in the substrate which do not support alumina formation, spallation of the scale either at temperature or under cyclic oxidation, the "pesting" phenomenon of substrate disintegration, and oxide embrittlement of the substrate, to name just a few of the more common problems. All of the aluminides with any potential for use as an engineering material have exhibited at least one if not all of the above phenomena. Extensive research into the oxidation of these materials, both as binary compounds and as the basis of alloys, has led to a reasonable understanding of oxidation

mechanisms. With this knowledge we can begin to modify the oxidation mechanism, either by alloying, surface modification, or a combination of the two.

The objective of this work is to investigate the application of a novel type of surface modification to the problems of oxidation exhibited by intermetallic compounds. Ion implantation of oxygen is used to form an oxygen saturated layer embedded in the surface of the materials. This approach is intended to form a continuous oxide layer at room temperature. The selective oxidation route to protective scale formation is thereby preceded by formation of a layer with a unique composition and structure produced by the implantation process. It is hoped that this structure may reduce the rate of dissolution of oxygen in the substrate and associated embrittlement. The layer formed by implantation is inextricably embedded in the surface and completely immune to spallation. It is a nonequilibrium structure which could potentially be more protective than the oxide initially formed by selective oxidation. If the structure formed by implantation is stable at high temperature, the presence of this layer may modify the scale growth mechanism as well as the kinetics, resulting in improved oxidation resistance during long term exposures. The use of the rare isotope ^{18}O provides a combined marker and tracer to help elucidate the effect of the implanted layer on the oxidation kinetics. Comparison with non-implanted specimens also provides information regarding the normal oxidation mechanism.

Three different compounds were chosen for this study, NbAl_3 , TiAl , and NiAl . These three compounds are among the most promising as the bases for engineering materials. Between the three of them they also exhibit all of the problems mentioned

above. This approach provides results of the effect of surface modification on a range of important problems. The results are also relevant to potentially useful material systems.

The objectives of this research therefore may be divided into three parts:

1) Determine the optimum ion implantation parameters which may result in the formation of an oxygen saturated layer in the target.

2) Determine whether the layer formed by ion implantation matches the calculated results and if in fact the implanted layer does consist of a continuous oxide layer at ambient temperature.

3) Study the stability of the implanted layer at high temperatures and determine what effects it has upon the oxidation kinetics and mechanism in the materials of interest. These results will be judged based on the present understanding of oxidation of these intermetallic compounds, as well as by comparison to control specimens which are not implanted or have been implanted with inert ions.

CHAPTER 2 REVIEW OF LITERATURE

Oxidation of NbAl₃, TiAl and NiAl

Oxidation of NbAl₃

NbAl₃ is a line compound with a melting point of 1680° C designated η in the Nb-Al phase diagram.¹ It is tetragonal with a c/a ratio of 2.24.² As a consequence of a limited range of solubility and complex crystallography, it is difficult to produce as a single phase material and has very poor mechanical properties. However the combination of high melting point, low density, and sufficient Al to form a protective scale makes it potentially valuable as the basis for engineering materials if the problems can be overcome.

Significant recent interest in NbAl₃ as a compound with favorable oxidation behavior started with Svedburg's³ report in 1976 where he observed that the slowest oxidation rate among Nb-Al alloys was exhibited by NbAl₃ at 1200° C. An inner layer of alumina was observed to form at the metal-scale interface while a layer of nonprotective AlNbO₄ formed at the oxide-gas interface. The parabolic rate constant k_p was reported to be 1.01 mg²/cm⁴ hr. This is commonly compared to the rate for NiAl which is about two orders of magnitude lower. (NiAl is generally used as a benchmark for oxidation rates of aluminide intermetallic compounds.) In the late 80s several independent groups worked on improving the oxidation of NbAl₃ by alloying additions. Perkins et al.⁴ pursued alloying with Ti and small additions of Cr and V. This did result in protective alumina formation at

high temperatures (1200-1400° C) at rates comparable to NiAl. The amount of Ti required for this improvement however results in a very complex microstructure. Furthermore the addition of Ti was reported to result in more rapid oxidation kinetics at 1100° C. The effects of microstructure on oxidation in this system were studied by Brady.⁵ Hebsur et al.⁶ pursued additions of 4 to 8% of Cr, Ti or Si with 1% Y or Zr. They also reported isothermal oxidation rates comparable to NiAl, as well as improved cyclic oxidation resistance, while maintaining the Al content at a level high enough to support an alumina layer at the scale-metal interface. The alloying elements in this case resulted in second phases rich in Si, Ti (as TiAl) or Cr. A later study by Doychak and Hebsur⁷ attributed the improvement imparted by Cr to the formation of a continuous layer of AlNbCr at the specimen surface, while the presence of Y improved the scale adherence on the Cr containing alloy by changing the scale microstructure.

The above studies concentrated on improving the high temperature oxidation of NbAl₃; however, the most severe oxidation problems occur at lower temperatures in this material. At temperatures between 650 and 1000° C and low oxygen partial pressures, NbAl₃ exhibits a disintegration phenomenon known as "pest".^{8 9 10 11} The terms "pest" or "pesteing" are used to describe oxidation at intermediate temperatures and low oxygen activities that result in the disintegration of the substrate material. This type of reaction occurs in numerous intermetallic systems. The state of recent papers on this phenomenon reflects a controversy over the precise mechanism of NbAl₃ pest. Pesteing in NbAl₃ was described by Aitken⁸ in 1967; however, no widely accepted mechanism for the phenomenon was described until 1989. Steinhorst and Grabke⁹ and Grabke et al.¹⁰

proposed that the pesting phenomenon was due to oxygen diffusion along grain boundaries and the resulting formation of alumina precipitates. It was suggested that the alumina precipitates in grain boundaries form a "crack opening wedge" that allows further oxygen penetration and eventually results in specimen disintegration. Due to the low solubility of O in NbAl_3 , this diffusion mechanism is still open to question however. In 1993 Topylgo and Grabke¹¹ proposed another mechanism for pest. In this paper they noted that aluminum transport through the material may occur preferentially along grain boundaries. This may result in the formation of Nb_2Al on grain boundaries with a consequent reduction in local volume. Due to the practically nonexistent elasticity of NbAl_3 , any internal stresses due to the local phase transformation may result in microcracks in both the metal and the scale. Oxygen may then travel down grain boundaries and form oxides which result in further cracking. This mechanism is also suggested to be applicable to pest phenomena occurring in any compounds with narrow ranges of homogeneity. No papers have as yet been published which test the predictions of this mechanism (pest rate related to grain size) at this writing. The question of mechanism involved in NbAl_3 pest is therefore still under investigation.

Oxidation of TiAl

The research into oxidation of TiAl often overlaps with that into NbAl_3 since just as Ti is added to Nb based alloys to improve mechanical properties, so is Nb often added to TiAl based alloys for the same reason. Single phase γ TiAl exhibits a homogeneity range however, unlike NbAl_3 . In the case of TiAl both of the constituents form oxides with

similar free energies of formation. This results in a competition between alumina and Ti oxide (primarily rutile) formation which varies with temperature and precise composition.

Welsch and Kahveci¹² and Meier et al.¹³ published surveys of oxidation in the Ti-Al system in 1989. Welsch and Kahveci noted that layered scales formed on γ grains and that in all cases an oxygen embrittled layer resulted underneath the scale. Meier et al. surveyed the oxidation kinetics of a range of Ti-Al compositions from 16 to 50 weight percent Al, in both dry oxygen and air. They observed alumina formation on γ TiAl at temperatures up to about 1000° C. A continuous alumina layer was not observed to form on any alloys falling outside of the γ phase field. They also ion implanted Al, Si, N, or C into a series of the same alloys. Surprisingly they observed accelerated oxidation in this case. They did not however offer any explanation for the accelerated oxidation in this particular report or any of their publications to date.

In 1992 Becker et al.¹⁴ published what is to date the definitive work on the oxidation mechanism in TiAl and γ based alloys. In oxygen exposures the key effect was determined to be the formation of oxygen embrittled Ti_3Al underneath the growing scale due to selective oxidation of Al. The mechanism of oxidation was observed to be controlled by a combination of outward cation diffusion and inward oxygen diffusion. The resulting scale consisted of an outer layer of coarse TiO_2 and a fine-grained inner layer of mixed TiO_2 and Al_2O_3 . Between these two layers a barrier layer of coarse-grained Al_2O_3 formed. With time however, the barrier layer dissolved and reprecipitated in the outer layer. This shift was associated with breakaway oxidation kinetics. The dissolution of a (semi) protective layer of alumina illustrates the difficulty of forming protective scales on

intermetallic compounds. A study of cyclic oxidation of the same alloys showed a similar mechanism which repeated due to scale spallation.¹⁵ These results are similar to those observed for unalloyed TiAl by Shimizu et al.¹⁶

Two recent papers report very interesting results which may result in further refinement of the accepted oxidation mechanism of TiAl. Beye and Gronsky¹⁷ report that two new phases were identified in the sub-scale region of TiAl oxidized in pure O₂ at 1000° C for durations up to 250 h. The formation of ternary Ti-Al oxides, identified as Ti₁₀Al₆O and Ti₁₀Al₆O₂ may be important to the mechanism of the non-protective mixed titania/alumina growth in the scale. In contrast Taniguchi et al.¹⁸ report that they have succeeded in forming protective alumina scales on TiAl which are stable under cyclic oxidation for more than 20 cycles (400 h) at 1300 K. This result was achieved by forming the scale by preoxidation at an extremely low oxygen activity provided by a pack of silica at 1200 K. This is particularly important to the current investigation in that it shows that protective scales may be formed on TiAl using unorthodox preoxidation techniques. The key to success in this case is to form a continuous alumina layer before any other oxide compositions are precipitated.

Oxidation of NiAl

The oxidation of β NiAl is easily the most extensively studied among all of the intermetallic compounds. The general oxidation mechanisms have been discussed in several excellent articles over the past thirty years. Due to its use as a coating extensive

literature exists on the cyclic oxidation of NiAl as well. Herein are reviewed some of the more recent articles.¹⁹⁻³¹

Oxidation of NiAl is characterized by two problems: transient oxidation and scale spallation. In this case the transient oxide consists of nonequilibrium aluminum oxide phases. Under cyclic oxidation the scale tends to spall to bare metal. Under isothermal oxidation however the scale formed at long times is more protective. Westbrook and Wood¹⁹ reported the occurrence and possible mechanism for pest in NiAl. Grabke et al.¹⁰ also identified the occurrence of pesting in NiAl; however, this phenomenon is reported to be much less severe than that exhibited by NbAl₃.

The transient oxides formed on NiAl are the γ and θ phases of alumina. At temperatures up to 1000° C these phases predominate during exposures of up to several hundred hours. In a TEM study of oxidation of single crystal NiAl, Doychak et al.³¹ observed that only θ alumina was present after 0.1 h at 1100°C. The formation of transient alumina phases is favored due to strong epitaxial relationships between the scale and the substrate metal. At longer times or higher temperatures the transient alumina phases transform to α alumina. This transformation starts at the gas/oxide interface and proceeds inward to the oxide/metal interface.^{20,21} The transformation to α alumina results in a reduction in volume of approximately 13%.²⁰ This volume change results in cracks in the scale which heal by outward transport of Al to form α alumina. These cracks produce a scale morphology characterized by circular ridges forming cells with further radial ridges within each cell. The more open structure of the transient alumina phases renders them less protective than α alumina. The transformation to α alumina has been used to account

for the discontinuous decrease in oxidation rate observed in NiAl at 1000° C and above.^{10,22} Several studies using ¹⁸O as a tracer have demonstrated that oxygen transport occurs primarily by the short circuit pathways present through the center of the ridges. Aluminum outward transport is also evidenced by the healed cracks protruding above the surface of the scale.^{23,24,25} This phenomenon is particularly evident in the high-resolution SIMS images presented by Prescott et al.²⁵ In this case both the outward diffusion of aluminum and the inward diffusion of oxygen along grain boundaries was demonstrated.

A number of studies have also investigated the effect of ternary alloying additions on the oxidation of NiAl. Zirconium in particular has been extensively investigated for its effect of improving the scale adherence of NiAl.^{22,26-28} The mechanism of improved scale adherence has never been clearly explained however phenomenologically Barrett²⁹ observed that the incorporation of ZrO₂ into the oxide layer may account for the improvement in scale properties. In the alloys containing Zr scales spalled near the scale/gas interface, rather than at the scale/metal interface as in pure NiAl. The improvement of scale adherence was postulated to be associated with gettering of tramp elements, particularly sulfur, however no direct evidence has been presented to support this hypothesis. Sulfur trapping is also one of the theories used to explain the effect of reactive elements such as yttrium in improving scale adherence on NiAl and other alumina forming alloys.^{23,24,30} This theory is contested by Grabke et al.¹⁰ however, who observed that sulfur segregates to the free surfaces of sub-scale voids formed on NiAl containing yttrium. Other major elements added to NiAl include Fe and Cr as major alloying elements and Ce and Hf as dopants.^{10,24,26} None of these elements has been observed to

dramatically improve the isothermal oxidation kinetics of NiAl beyond that obtained at 1000-1100° C once an α alumina scale has formed however.

Summary of Oxidation Studies

The oxidation mechanisms of all three of the alloys chosen for this study have been thoroughly investigated. Although some questions remain regarding the specifics of oxidation mechanisms, it is possible to describe the key problems with each alloy: NbAl₃ suffers from a very narrow range of aluminum solubility. Although continuous alumina scales may form on NbAl₃, they fail due to the formation of less favorable phases (particularly Nb₂Al) beneath the scale and possibly along grain boundaries. The pesting phenomenon may be related to the dissolution of oxygen in the substrate and/or the formation of second phases along grain boundaries. TiAl also forms continuous alumina scales at high temperatures. Although the solubility range of TiAl is fairly broad, loss of aluminum may result in the formation of α_2 Ti₃Al beneath the scale. This phase has a high solubility for oxygen and is easily embrittled. The free energies of formation of TiO₂ and Al₂O₃ are also very similar. This results in a competition between formation of alumina and less protective titanium oxides. The oxygen affinities of Ti₃Al and lower titanium oxides are sufficiently high that in the presence of these phases, alumina already formed may be reduced and reform on the outside of the scale. A treatment which favors the formation of aluminum oxide may be used to improve the oxidation kinetics of TiAl. NiAl suffers from poor scale adherence and exhibits a pesting phenomenon. The formation of less protective transient alumina phases is primarily responsible for the problems exhibited

by NiAl. This makes the possibility of developing a surface treatment which changes the initial oxidation mechanism of NiAl attractive. Between these three alloys most of the major types of problems in oxidation of intermetallics are exhibited.

Effects of Ion Implantation on Pure Metals and Alloys

Both equilibrium and metastable phases may be produced by ion implantation. In all cases however the phase distribution is unique. A general overview of phase formation in implanted metals is provided by Follstaedt.³² Ion implantation is a surface modification technique which is limited to a maximum depth (depending on accelerator energy) of 1-2 μm . In this shallow layer however it is possible to create structures with properties significantly different from the bulk material. The phase changes induced by inert ion irradiation may result in crystalline or amorphous phases. Ordered phases or intermetallic compounds may also be formed as a result of implantation. By implanting reactive species it is also possible to precipitate phases with a composition similar to equilibrium phases, but possessing a microstructure unique to the implantation process. It is this last effect which is of particular interest to this study.

Pure Metals

Oxygen implantation has been used extensively to form oxide layers in silicon. The application of this process to the fabrication of electronic devices is referred to as Simox. (Separation by Implanted OXygen).³³ A very extensive literature relating to Simox has been published since it was first described in 1978. In addition to electronic measurements

the properties of Simox layers are commonly studied using RBS (Rutherford backscattering spectroscopy), SIMS (secondary ion mass spectrometry), AES (auger electron spectroscopy), and XPS (x-ray photoelectron spectroscopy, also known as ESCA), as well as TEM (transmission electron microscopy). These techniques can also be applied to the analysis of phases formed due to the implantation of alloys. The effects of oxygen implantation on pure metals and alloys are reviewed below. The Simox process is discussed in numerous reviews such as the one by Wilson.³³

Perkins et al.³⁴⁻³⁶ were among the first to report formation of aluminum or titanium oxide due to the implantation of oxygen. The targets used in this study were thin films (200-500 Å) vapor-deposited on glass or silica substrates. The primary focus of their work was on forming electrically insulating thin films. TEM examination revealed a microstructure consisting of polycrystalline and amorphous regions. In aluminum the structure consisted of polycrystalline islands of residual Al in an "amorphous dielectric matrix." In titanium the structure consisted of a mixture of crystalline TiO and amorphous Ti_xO_y (possibly TiO_2). Although these studies demonstrated the ability to form Al and Ti based oxides by ion implantation, the choice of thin film targets makes it likely that the particular microstructures formed are not representative of those observed in bulk material. A later work by Chereckdjian and Wilson³⁷ on evaporated thin films of Al found contradictory results. In this case the oxide was found to be polycrystalline, stoichiometric Al_2O_3 . Using a combination of TEM, RBS, and XPS, it was determined that the oxygen concentration saturates at a dose of 9×10^{17} O ions/cm² at 100 keV. At a dose of 1.8×10^{18} a continuous oxide layer was formed which intersected the sample surface.

XPS confirmed that as the dose increased the signal due to metallic Al decreased while that due to alumina increased. Yadav and Bhatia³⁸ studied the electrical properties of a similar implantation synthesized film. They found that the ordered alumina structure formed by implantation had an electrical resistivity comparable to that synthesized by any conventional technique. Therefore the oxide layer formed by implantation of pure aluminum was concluded to be continuous stoichiometric Al_2O_3 .

The first study to be reported on oxygen implantation into bulk aluminum was that of Musket et al.³⁹ They implanted polycrystalline Al foils at oxygen fluences of 1 to 16×10^{17} ions/cm² and observed formation of continuous alumina at doses in excess of 8×10^{17} . The oxide layers were characterized using RBS and Auger spectroscopy. In specimens exposed to the higher fluences they also observed the formation of oxygen bubbles.⁴⁰

A group of investigators at Sandia national laboratories have published several papers on oxygen implantation of aluminum.^(6 & 41-43) Myers and Follstaedt investigated the trapping of Deuterium in oxygen implanted aluminum.⁴¹ In these experiments polycrystalline specimens were implanted with a dose of 1×10^{17} O/cm². TEM examination did not show any evidence of oxide formation in as-implanted specimens. In specimens which were first implanted and then annealed at 873 K, precipitates of γ alumina were observed. The cubic γ alumina was observed to precipitate with its cubic axes parallel to those of the aluminum matrix. Deuterium trapping was observed in both as-implanted and annealed specimens. This lead them to speculate that O clusters were formed in the as-implanted specimens, with no particular structure. Bourcier et al.⁴² examined

mechanical properties of oxygen implanted aluminum. In order to produce a continuous implanted layer from the surface to a depth of 500 nm, a series of different implants were performed at fluences ranging from 0.5 to 2×10^{17} ions/cm² and accelerating energies from 25 to 200 keV. The implanted specimens were then characterized using TEM and RBS. They also observed γ alumina precipitates in specimens which had been annealed at 450-550° C. In 1991 Follstaedt, Myers, and Bourcier⁴³ published a detailed TEM study of the microstructures of non-annealed aluminum foils implanted at room temperature. In this study, using doses similar to those in the previous studies, they identified oxide precipitates in the as-implanted aluminum. These were identified as a disordered version of the γ alumina phase, with precipitate dimensions of 1.5-3.5 nm.

Oxygen (and nitrogen) ion implantation into Al has also been investigated by Ohira and Iwaki in Japan.^{44,45,46} They also observed precipitation of γ alumina. At high doses (up to 4×10^{18} ions/cm²) they observed formation of continuous alumina layers. The γ alumina layer, once formed, was determined to be stable under continued irradiation. Implantation of nitrogen was likewise determined to result in stoichiometric AlN. The objective of all of this work was reported to be the synthesis of insulating layers for electronic applications. None of the above studies involved any type of subsequent corrosion experiments.

In addition to the investigations mentioned above, there have been a few papers which report the results of oxygen ion implantation solely into pure Ti. Stroud⁴⁷ studied the effects of strain on oxygen ion implanted Ti. The implantation was reported to result in the formation of a cermet of Ti metal and oxide, similar to Perkins³⁵ results. Fifteen years

later Okabe et al.⁴⁸ reported the formation of rutile by high-dose implantation of oxygen. At doses greater than 1×10^{18} they determined that only stoichiometric TiO_2 in the rutile structure, was present. This was observed in as-implanted specimens by XPS and XRD. A later study⁴⁹ showed that while TiO_2 was formed by room temperature implantation, at -60°C TiO was formed. This could be converted to TiO_2 by further implantation at room temperature however. The orientation of the rutile formed by implantation was shown to be affected by the energy of the implanted ions as well as the temperature.

The above investigations may be summarized as follows; the implantation of oxygen or nitrogen into pure, polycrystalline, Ti or Al results in stoichiometric polycrystalline oxides or nitrides. Once the dose required to form the oxide is reached, the phase is stable under further irradiation. The crystal structure and grain size of the phases formed are unique to the process by which they were created. It is particularly important to realize that these oxide or nitride layers do not form a distinct interface with the metallic substrate. The implantation process produces layers buried in the surface of the target, at the edges of which are relatively broad regions containing a gradient in defect concentration and implanted atoms, but no precise edge. Consequently the implanted layer should be immune to spalling or separation from the substrate, even under temperature cycling.

Implantation of Alloys and Oxides

No studies involving oxygen implantation into alloys of Ti, Al, Ni, or Nb were discovered in this literature search. The only relevant studies of oxygen ion implantation

are those involving pure metals which are discussed above. There are however numerous published studies on the effect of inert ion bombardment of alloys and intermetallic compounds. The objective of most of these studies is to study nonequilibrium phase formation induced by ion beam mixing. The phases produced by inert ion bombardment range from ordered compounds to amorphous structures. Oxygen implantation results in a combination of ion beam mixing due to ballistic processes, and the formation of new phases due to the high concentration of oxygen introduced into the specimen. The structures produced due to inert ion implantation of the phases covered in this study are therefore relevant, insofar as they reflect the irradiation effects of oxygen implantation.

Of the materials of interest to this study, the nickel-aluminum system has received the most attention. This is apparently due to the different ordered structures available in the Ni-Al system, which may exhibit a range of responses to irradiation. Brimhall et al.⁵⁰ surveyed the effect of self-ion (implantation of a species which is a component of the substrate) implantation (2.5 MeV Ni⁺) on a series of intermetallic compounds, including NiAl, Ni₃Al, and NiAl₃. NiAl and Ni₃Al were found to remain crystalline, while NiAl₃ transformed to a partially amorphous microstructure. NiAl was found to be particularly radiation resistant, with distinct long range order after high ion doses. A high density of defect clusters (possibly dislocation loops) was produced in both the NiAl and the Ni₃Al. Based on the results of this study they proposed a criterion for amorphous phase formation, based upon the range of solubility exhibited by the original phase. Small compositional ranges or limited solubility in the phase field of the target were associated with amorphous phase formation. A contrasting study was conducted by Hung et al.⁵¹

wherein vapor deposited layers of pure metals were irradiated with inert heavy ions (500 keV Xe). In this ion beam mixing study, NiAl was produced from the vapor deposited layers. When the layered structure was annealed to produce intermetallic phases prior to implantation, NiAl was once again found to be stable while NiAl₃ converted to a partially amorphous structure. Here the conclusion was that amorphous phases are associated with complex crystal structures in the target. In a similar study focusing solely on NiAl, Delafond et al.⁵² once again showed that at room temperature NiAl was produced by irradiation of Ni-Al layered films. They also showed that an amorphous structure could be produced by irradiation of the crystalline material at 77 K. The amorphous structure transformed back to the ordered structure after further irradiation at room temperature. More complex crystal structures were observed upon annealing the amorphous phase. This study was followed up by determining the temperature dependence for amorphization of NiAl.⁵³ It was determined that at very low temperatures (4K) amorphization is due to a direct ion impact mechanism. As the temperature increases, thermally activated heterogeneous crystallization competes with the amorphization process. Above 120 K complete amorphization cannot be achieved with Xe bombardment and this critical temperature decreases as the ion mass decreases. Kyllesbech et al.⁵⁴ conducted a very similar study over the entire composition range of Ni-Al. Once again their results showed that NiAl is not amorphized by room temperature irradiation. They performed thermodynamic modeling, using a combination of equilibrium and metastable approaches, to predict amorphous phase formation. This approach proved to be only partially successful however, as all the crystalline phases with simple crystal structures were

predicted to occur, in contrast to the experimental results where only β NiAl was observed. Eridon et al.⁵⁵ modeled the results of a similar series of experiments using a combination of thermodynamic and kinetic approaches. They implanted both polycrystalline and layered specimens of Ni-Al alloys with 500 keV Kr ions. The phases observed included ordered and disordered crystalline structures and amorphous regions. Using the embedded atom method to model the structures and calculate heats of formation, they concluded that metastable states with moderate heats of formation, near that of the stable phase, were likely to form under irradiation, while those whose heats of formation were around 50% or less that of the stable phase, were not likely to form. The persistence of the ordered state in irradiated NiAl at room temperature was attributed to radiation enhanced diffusion, which cancels out the disordering due to irradiation.

Ahmed and Potter⁵⁶ studied the effect of implanting aluminum into pure polycrystalline nickel. Implanted concentrations reached up to 75% Al. In this case the only intermetallic phase formed was NiAl. In the place of Ni_3Al , an hcp phase was observed. The NiAl formed at implanted fluences up to 2×10^{18} ions/cm² exhibited a Nishiyama relationship with the FCC substrate. This was taken to indicate that the NiAl was formed by a martensitic reaction, although some short-range diffusion is required. The driving force for the martensitic reaction is assumed to be the stress built up in the implanted layer. At the highest doses an amorphous phase containing random islands of NiAl was observed. At fluences above 8×10^{17} ions/cm² the observed dislocation density in the precipitated β phase decreased until no dislocations were visible at fluences of 2.4×10^{18} and above. The disappearance of dislocations was speculated to be due to the ability of the

NiAl to retain a high density of aluminum vacancies. This may then allow rapid dislocation climb to the surface while rapid recombination of interstitials prevents the formation of new vacancies. Another proposed mechanism involved the high concentration of crystallite (grain) boundaries, which could act as point defect sinks.

Implantation of TiAl or NbAl₃ has received far less attention than NiAl. No studies involving oxygen implantation of TiAl were found however there have been three different reports of nitrogen implantation into TiAl. Saito and Matsushima⁵⁷ implanted polycrystalline TiAl at up to 5×10^{17} ions/cm². They reported that surface hardness increased by a factor of 3. This result was attributed to a combination of solid solution hardening by dissolved nitrogen, formation of TiN_x precipitates, and radiation hardening by point defects. Was⁵⁸ also studied the hardening of nitrogen implanted TiAl at doses of 1.2 to 36×10^{16} ions/cm² at 200 keV. No microstructural analysis was performed but he observed results similar to those of Saito and Matsushima. Boerma and Corts⁵⁹ implanted nitrogen into bilayers of Ti and Al evaporated onto a Si substrate. They observed that the nitrogen was trapped by both Ti and Al. In this same study they also implanted Ni-Al specimens and observed nitrogen distributions which indicated preferential trapping by aluminum.

Saqib and Potter⁶⁰ studied phase formation in aluminum implanted niobium. Several interesting observations were made in this work. A range of implantation doses was used which resulted in aluminum concentrations of up to 70 at. %. At fluences up to about 1.6×10^{18} ions/cm², the surfaces of the implanted specimens were observed to remain shiny and exhibit no irradiation induced topography. At higher doses roughening occurred

with oscillations of around 500 Å. None of the intermetallic phases were observed. The solubility of the BCC Nb structure was extended up to an ion dose of 1.6×10^{18} ions/cm² (resulting in an Al concentration of approximately 60 at. %). At higher fluences a microcrystalline phase formed followed by an amorphous structure. This was rationalized in terms of the free energy difference between the liquid phase and disordered NbAl₃. The amorphous phase was observed to possess short range order associated with NbAl₃. The presence of this (short range) order was postulated to reduce the free energy of the liquid below that of the intermetallic phase. In the same study parallel results were observed in Ta.

Pampus et al.⁶¹ investigated the formation of metastable phases in the Nb-Al system using ion-beam mixing. Layered thin films with average compositions from 20 to 85 at.% Al were implanted with 500 keV Xe ions at a dose of 2×10^{16} ions/cm² and temperatures from 40 to 620 K. Other than the above mentioned BCC solid solution and the amorphous phase, the only crystalline phase observed was NbAl₃ at an irradiation temperature of 623 K. A calculated metastable phase diagram was compared to the results of the experiments. It was concluded that metastable equilibrium is achieved during ion-beam mixing. The formation of the ordered phase at elevated temperatures was attributed once again to radiation enhanced diffusion.

Finally, since the objective of this study is to form aluminum oxide by ion implantation, it is appropriate to review the effect of ion implantation on alumina. McHargue et al.⁶² reviewed the work performed on implantation of alumina up to 1984 and presented additional data of their own utilizing several ion species (Cr, Zr, Nb, Xe and

Al+O) over a range of temperatures and fluences. All of the specimens they implanted at room temperature exhibited color centers attributed to electrons trapped by oxygen vacancies. Implantation of Al and O in a ratio of 2:3 at 77 K resulted in the formation of an amorphous layer 150 nm thick. Zr implantation resulted in formation of an amorphous layer at room temperature. This result was not obtained with any of the other species however. In a following study on annealing of implanted oxides, White et al.⁶³ determined that the amorphous alumina layer produced by (Al +O) implantation recrystallizes as γ alumina then transforms to α alumina. The γ - α transformation occurs along a clearly defined interface. The transformation to γ alumina took a few minutes while the subsequent transformation to α alumina proceeded over several hours at 960° C. Interestingly this behavior is similar to the transformation of the transient oxides in NiAl to α alumina. Based on the velocity of the α/γ interface they determined an activation energy for the γ - α transformation of 3.6 eV/atom. Zinkle⁶⁴ studied the effect of simultaneous triple ion bombardment (Al, O, He) at room temperature on the microstructure of polycrystalline alumina. The substrate in all cases remained crystalline. Four types of radiation-induced defects were produced in the specimens. The most significant of these was a high density of dislocations. Small cavities were produced which were attributed to the He implantation and defect clusters were observed which were postulated to be Al "colloids" since Al had been implanted in excess of stoichiometry. Ramos et al.⁶⁵ investigated the effect of Ti ion implantation at 300 K on single and polycrystalline alumina. Using RBS they determined that in both materials an amorphous layer was produced at a fluence of 1×10^{17} ions/cm². The implanted Ti was determined using XPS to

exist in the Ti^{+3} state near the surface and in both the Ti^{+3} and the Ti^0 metal state near the peak of the implanted distribution.

Summary of Ion Implantation Literature Review

The literature on ion implantation of metals and alloys suggests several broad conclusions: First, it is possible in pure materials to form stoichiometric oxides. Rutile may be formed on Ti and various alumina allotropes may be precipitated on Al substrates due to implantation of oxygen. Consequently the formation of a continuous oxide layer on intermetallic compounds implanted with oxygen may occur. In the case of TiAl there is likely to be formation of a mixed oxide containing roughly equal proportions of oxidized Ti and Al. No studies were found involving implantation of Ni with oxygen; however, in NiAl and NbAl₃ the lower free energy of formation of alumina may favor formation of primarily aluminum oxide from the implanted oxygen over compositions containing Nb and Ni in anything close to an equilibrium composition.

Second, the wide variety of microstructures obtained on pure materials prepared by different methods makes it impossible to accurately predict the structure of the oxide layers formed by oxygen implantation of intermetallic compounds. What can be said however is that the structure is bound to be unique to the particular composition of the substrate. The stability of NiAl, NbAl₃ and alumina under inert ion irradiation suggests the possibility that the crystal structures of the substrates will be maintained for as long as they can accommodate the implanted oxygen within the lattice. As the oxygen implant is built up, the fraction of the target region which is oxidized may increase, gradually resulting in

an oxide layer whose structure and elemental composition reflects the displacements in the original host lattice produced by the implantation process itself. Finally, despite the number of investigations into oxygen implantation into metals, the almost complete lack of oxidation studies of oxygen implanted metals in general and intermetallic compounds in particular makes this study particularly timely.

CHAPTER 3 EXPERIMENTAL TECHNIQUES

Materials Preparation

The materials to be used in this investigation were chosen on the basis of their technological importance, demonstrated ability to form alumina scales, and their utility in demonstrating the effects of oxygen implantation. Two different sources provided the materials used. The NbAl_3 and TiAl were obtained as arc-melted ingots weighing approximately 250 grams from United Technologies (Pratt & Whitney, West Palm Beach, Florida). The NiAl was obtained as high-purity single-crystal wafers produced in the Materials Science and Engineering department at the University of Florida by Dr. Vladimir Levit. The NbAl_3 as-cast is essentially single-phase (η) as determined by electron microscopy, x-ray diffraction, and electron microprobe. Insofar as NbAl_3 exhibits an extremely narrow range of solubility this is a tribute to the skill of the technicians at Pratt & Whitney. Although porous and extremely brittle this was considered acceptable for the experiments planned in this investigation. The TiAl is nearly stoichiometric Ti-50Al . The as-cast microstructure contains a mixture of γ and α_2 phases. The TiAl was heat treated at 1200°C for 4 hours and oil quenched to obtain a single phase γ microstructure. The NiAl is near exact stoichiometry. It was provided as EDM sliced wafers oriented near $[100]$, $[110]$ or $[111]$.

Specimens of TiAl and NbAl₃ were sectioned using a low-speed diamond saw to produce rectangular specimens approximately 1-3 cm. on a side and 1 mm (in the case of TiAl) to 3 mm (NbAl₃) thick. These specimens were then ground and polished using standard metallographic techniques to a 1 μ m finish followed by a final polish of 0.03 μ m (colloidal silica). Because these specimens were intended for SIMS analysis, which ideally requires a smooth, homogeneous surface, no etch was used and polishing relief was minimized as much as possible. The NiAl specimens were heavily ground in order to remove surface damage due to EDM. They were subsequently polished to a 1 μ m (diamond) finish.

Ion Implantation

All of the ion-implantation was performed at the surface modification and characterization facility at Oak Ridge National Laboratory (SMAC-ORNL). Implantation parameters were modeled using the PROFILE code.⁶⁶ The actual implant doses used were subject to practical limitations, in particular the accelerating energy and maximum current available from the implanter. The Varian-Extrion implanter used is designed to provide accelerating energies for singly charged ions of up to 200 kV. In practice however the upper limit is 160-170 kV depending on the ion being implanted. The beam current available also varies with the ion chosen for implantation. It is relatively easy to obtain high ion currents of oxygen. These experiments required ion doses 2-3 orders of magnitude higher than those normally used in electronic materials. Consequently the maximum dose was limited by the time required for each implantation since available beam

time at SMAC was limited. In general the specimens were implanted at accelerating energies of 35 to 164 keV at doses from 1×10^{17} to 1×10^{18} ions/cm². The results discussed herein focus primarily on the specimens implanted at the higher doses and accelerating energies. The specifics of implantation into each material are covered in the results chapters.

Test Environments

Five different atmospheres were utilized in this investigation: Air, Argon-0.1% O₂, Ar-50ppm O₂, high purity argon, and Ar-4.62 % H₂. These atmospheres were utilized to achieving strongly oxidizing, weakly oxidizing, pesting, inert, or reducing conditions. Argon-oxygen mixtures were used in order to avoid complications due to reactions with nitrogen. The 1000 ppm (0.1%) oxygen concentration was initially chosen to reduce the rate of oxygen uptake below that seen in air. In practice however this environment is very nearly as oxidizing as an atmospheric concentration of oxygen. The Ar-50 ppm O₂ mixture was used primarily to induce "pesting" in the NbAl₃ specimens to determine if this phenomenon was affected by the presence of an oxygen implanted layer. The high purity argon environment was used for annealing implanted specimens, in order to study the stability of the implanted layer in the absence of continued oxidation. The Ar-H₂ mixture was also used as an annealing environment since, in order to completely avoid oxide formation on these alloys, an oxygen activity far lower than that achievable in high-purity inert gases is required.

All of the exposures were conducted at 1000° C. At this temperature all three alloys may be expected to form alumina oxide layers. The results obtained at 1000° C may be extrapolated to higher and lower temperatures based on the current understanding of oxidation in these intermetallic compounds. Therefore varying the exposure temperature was deemed an unnecessary complication which would not add to understanding the effect of oxygen implantation on the oxidation mechanisms. Furthermore the limited availability and expensive preparation and analysis of the implanted specimens, demanded that the maximum amount of information possible be extracted from the minimum number of experiments.

Analytical Techniques

Specimens were analyzed thoroughly before implantation, as implanted, and after annealing or oxidation treatments. In order to minimize error due to variations in instruments and techniques, as much as possible implanted and non-implanted areas of the same specimens were used for comparison. The primary techniques utilized were Auger electron spectroscopy (AES) and secondary ion mass spectrometry (SIMS). Additional data were obtained from x-ray diffraction (XRD), x-ray photoelectron spectroscopy (XPS), electron microscopy (SEM), and optical microscopy. The specific applications of these techniques are discussed below. Ironically perhaps for an oxidation study, thermogravimetric analysis (TGA) was of very limited value. Most of the specimens used in this study were only implanted on part of one side; therefore, the results of TGA show an unbalanced average between "ideal" non-implanted and implanted specimens.

Furthermore, since short exposure times were used for many of the experiments, the accuracy of TGA was poor due to the low net weight gains involved. TGA did prove valuable for monitoring the process of pesting in the NbAl₃ however.

Auger Electron Spectroscopy

AES was used primarily to characterize as-implanted specimens. In general Auger spectroscopy acts as a sensitive microprobe for semi-quantitative analysis of the composition and (in conjunction with inert ion sputtering) depth distribution of elements in thin near-surface layers. In some cases, notably that of Al, the ionization state of the elements can be inferred from shifts in the position of the characteristic Auger electron peak energies. In the case of Ti there are differences in peak shape between the metal and oxide. In the case of Ni and Nb, however, the differences between oxide and metal signals are much more subtle and were not of practical value in this study. The use of Auger spectroscopy therefore allowed the identification of some of the oxides formed by ion implantation. However not all of the possible species could be clearly identified.

Secondary Ion Mass Spectrometry

SIMS was used as the primary instrumental technique in this study. In dynamic SIMS a small selected area of the specimen is bombarded with ions in order to provide a depth profile of the near-surface region. The material sputtered from the surface is in the form of neutral particles, or positive or negative ions. The secondary ions may be either monatomic or molecular. Either positive or negative ions may be collected in the SIMS.

The ionization yield, and in some cases the charge of the resulting ions of a particular species, depends on the ion and accelerating energy used for the primary ion beam. The rate at which a particular specimen sputters depends on the chemical composition of the surface. This of course will change if layers of different composition are being sputtered through. The absolute relationship of the collected secondary ion current to the atomic composition, therefore, depends on a combination of all of the above variables as well as the surface topography of the specimen and the collection efficiency of the detector. In order to minimize these variables the following approach was used: In all cases implanted and non-implanted regions of the same specimen were analyzed using the same instrumental settings. Measurements were repeated at several different equivalent regions of a particular specimen. All of the measurements for a particular specimen were made on the same day in order to keep instrumental variability to a minimum. Only polished specimens were used with a minimum 1 μ m surface finish. Oxidized specimens for SIMS analysis were only exposed for short times in order to minimize the oxidation induced surface topography. Consequently the SIMS data presented herein is intended primarily for comparison to spectra obtained from the same specimen. This does not represent a significant limitation on the results obtained in this study however.

All of the SIMS analysis was performed on a Perkin-Elmer PHI 6600 spectrometer. Cs⁺ ions at 7 keV were used for sputtering. The beam was rastered over an area on the specimen of either 200x200, 300x300, 400x400, or 550x550 microns, depending on the specimen condition. The ion current used varied from 100 to 900 micro amps, also optimized for the particular specimen. In order to avoid what is termed "crater

wall effects" a 12% electronic gate was used. This means that in order to avoid collecting ions sputtered from the edge of the sputter pit, which would raise the background count rate in some species, the secondary ions were only collected from the central 12% of the sputter pit. This is achieved by gating the signal from the mass spectrometer with the position of the primary ion beam. In this investigation oxygen and oxide species were of primary interest; therefore, negative ions were collected in most cases. Specific aspects of the depth profiles are discussed in the results sections below.

X-Ray Diffraction

XRD was used primarily to determine if significant amounts of a crystalline phase was precipitated in any of the implanted samples. Specimens were scanned using a powder diffractometer (Phillips APD 3720) in as-implanted, annealed, and oxidized conditions. Based on the available literature, the possible phases included, in addition to the substrate patterns, rutile (in TiAl) and possibly γ alumina or another metastable alumina phase. In order to maximize the available instrumental sensitivity, very low scan rates were used over selected regions where peaks for the possible precipitate phases would appear. Because the implanted layers thin, amorphous phases or those existing as a sparse distribution of fine crystallites in a matrix possessing only short range order, were not expected to produce any measurable intensity against the substrate background. In the latter cases transmission electron microscopy might be able to identify the structure of the implanted layer. However, in light of the fact that this study is concerned with brittle intermetallic materials which are very difficult to prepare as cross-sectional TEM

specimens and that the primary interest lies in examining the effects on oxidation kinetics due to the implanted layer, whatever form it may take, TEM examination was deemed outside the scope of the present work.

Microscopy

Both SEM and optical microscopy were used to examine selected specimens in plan and cross-sectional views. Alloy microstructures were enhanced by etching with a modified Kroll's reagent. Since the specimens were required to be as smooth as possible for SIMS analysis the implanted specimens were not etched. In all cases the specimens were mirror polished single phase material so that very little topography was visible in either SEM or optical microscopy prior to oxidation. In the end, although all of the specimens were thoroughly examined, microscopy proved to be of relatively little value to this study. This may be simply explained by the extremely fine microstructure produced by implantation. The implanted surfaces often exhibit differences in color or reflectance which are visible with the naked eye. These differences are due to the aggregate effects of differences in surface topography or scale thickness on too fine a scale to clearly discern in an SEM however. Consequently macro photography was used to produce illustrations of the appearance of selected samples. SEM was useful in those few cases where significant topographic variations occurred.

X-Ray Photoelectron Spectroscopy

XPS was used to determine the oxidation states of elements near the surface of the specimens. This was particularly valuable in the as-received and in the as-implanted

specimens for determining the surface oxidation states which could be correlated to the results observed in SIMS and Auger depth profiles. Much of the preliminary work for this investigation involved XPS. Due to the poor depth resolution of XPS however, analysis of the oxidation states present in the implanted layers was solely by Auger spectroscopy.

CHAPTER 4 OXYGEN IMPLANTED NbAl₃

Ion Implantation

As a practical limit the maximum dose used for all of the implants in this study was 1×10^{18} ions/cm². This limit was dictated by the maximum current of ¹⁸O available in the ion beam using the Varian Extrion 200 kV implanter at SMAC-ORNL. In the initial experiments it took approximately three hours to implant an area of 10 cm². As this project progressed improvements in the implanter and further experience with ¹⁸O beams shortened the time required to reach the maximum dose to approximately 90 minutes. The objective of the implants was to obtain a sufficient concentration of oxygen in the implanted specimen such that a continuous layer of 2:3 metal:oxygen ratio, or M₂O₃ stoichiometry could be formed. It was assumed that sufficient oxygen is implanted to combine with all of the available aluminum if a peak concentration of 0.6 times the Al concentration in the target alloy is achieved. Although this clearly results in an implanted region which contains insufficient oxygen to combine with all of the available metal atoms, in order for a layer to form which consists of continuous Al₂O₃ additional aluminum atoms must diffuse into the implanted layer and the other metal, Nb in this case, which remains in the implanted layer must either be dissolved in the oxide or diffuse out to the surface to form a separate oxide layer.

Modeling using the PROFILE code indicated that at a dose of $1 \times 10^{18} \text{ }^{18}\text{O}$ ions/cm² and an accelerating energy of 170 keV a peak concentration of 45.2 % oxygen could be reached with the implanted layer extending from near the surface to a depth of 400 nm. If the oxygen was preferentially trapped by Al a concentration of 45% would result in continuous Al_2O_3 (containing significant amounts of Nb metal). The calculated profile is shown in fig. 4-1. In order to reach a concentration of closer to 60% O a dose on the order of five times greater would be required. It would also be possible to form a thinner layer closer to the specimen surface using lower accelerating energies. However this results in increased surface sputtering and decreased retention of the implanted species due to the intersection of the implanted distribution with the surface. This phenomenon is illustrated in the implanted profile of fig. 4-2 which shows the calculated result of an implantation at 100 rather than 170 keV. The peak concentration is nearly as high but the retained dose in this case is 69.2% vs. 98.3% for the higher dose. A series of implants were performed at 100 keV however, in order to determine the effect of changing the initial implanted distribution. In order to investigate the effects of radiation damage due to implantation three specimens were implanted with $1 \times 10^{18} \text{ }^{20}\text{Ne}$ ions/cm² at 160 keV. (The lower accelerating energy was used due to prevailing conditions on the day of the implantation.) The calculated profile for this implant is shown in fig. 4-3.

The calculated sputtering loss from the Ne implant is only slightly higher than that for the equivalent O implant. Qualitatively however there appeared to be considerably more surface loss in the Ne implants than in oxygen implants. In the case of oxygen all of the specimens appeared to be unchanged after implantation. There practically no change in

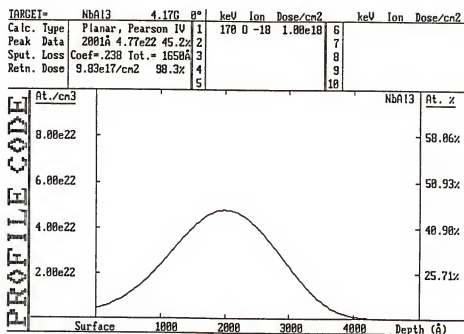


Figure 4-1. The calculated oxygen distribution obtained using the PROFILE code for implantation of 1×10^{18} ^{18}O ions/cm² at 170 keV into an NbAl₃ target. The maximum concentration of oxygen obtained is 45.2%.

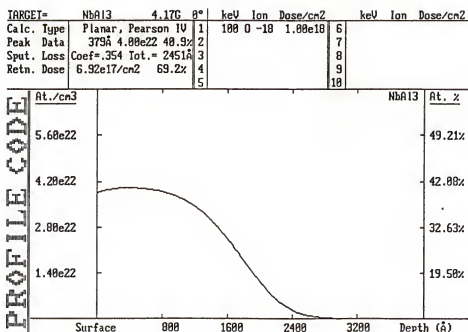


Figure 4-2. The calculated oxygen distribution obtained using the PROFILE code for implantation of $1 \times 10^{18} \text{ }^{18}\text{O}$ ions/cm² at 100 keV into an NbAl₃ target. The maximum concentration of oxygen is 40.9 %. The oxygen distribution intersects the surface of the specimen but the retained oxygen dose is only 69.2% of the incident ions compared to the 98.3% retention obtained at 170 keV.

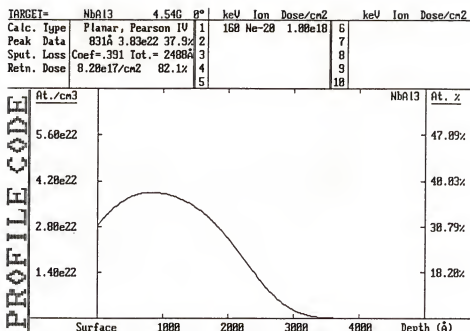


Figure 4-3. The calculated oxygen distribution obtained using the PROFILE code for implantation of $1 \times 10^{18} \text{ }^{20}\text{Ne}$ ions/cm² into an NbAl₃ target. This implant was performed to model the effects of radiation damage on the target. The Ne implant resulted in much more surface damage than the oxygen implant however.

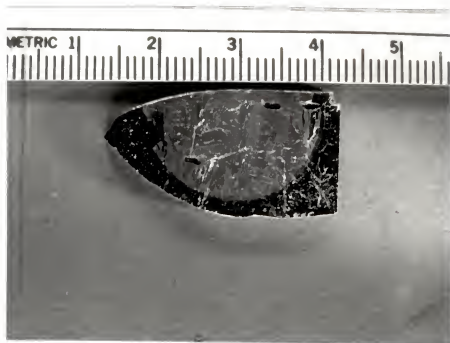


Figure 4-4. Macrograph of a Ne implanted specimen of NbAl₃. Note the frosted appearance of the implanted specimen region. This type of surface damage was not observed on the oxygen implanted specimens.

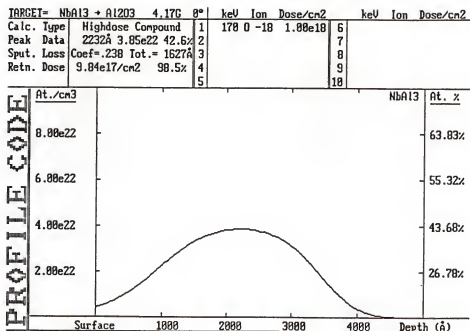


Figure 4-5. The calculated oxygen distribution obtained using the PROFILE code for implantation of 1×10^{18} ^{18}O ions/cm² into an NbAl₃ target assuming that the implanted oxygen forms alumina during the implantation process.

the surface finish and it was not possible to measure a step between the implanted and unimplanted regions using a profilometer. (Dektak). The Ne implanted specimens on the other hand appeared to have been etched or frosted by the implantation. A macrograph of a Ne implanted specimen is shown in figure 4-4. The lack of apparent surface damage in the O implanted specimens was the first result which indicated that compound formation was occurring due to oxygen implantation. The effective coefficient for oxygen sputtering appears to have been reduced due to trapping of the oxygen in the substrate. This result also indicates that the calculated profiles do not accurately reflect the actual implanted distributions obtained with oxygen. Note that the calculated profile in figure 4-1 predicts a sputter loss of 1650 Å from the surface of the specimen. This clearly did not occur. Compound formation could contribute to reduced sputtering losses from the surface. The PROFILE code can account for binary compound formation. A calculated profile for NbAl₃ implanted with 1×10^{18} ¹⁸O ions/cm² at 170 keV, and assuming that the implanted oxygen forms Al₂O₃ is shown in fig. 4-5. In this case a significant amount of surface sputtering (1627 Å) is still predicted however. Consequently the calculated profiles are regarded as a semi-quantitative predictor of the actual implanted distribution.

Oxidation and Annealing Treatments

Two different types of oxidation behavior are of interest in NbAl₃. The "normal" high-temperature oxidation regime consists of oxygen activities near that of the atmosphere and temperatures above 800° C. The "pesting" regime occurs at lower temperatures and very low oxygen activities. The "normal" oxidation experiments were

conducted at 1000° C in an atmosphere consisting of 0.1% O₂ in high purity Ar. This atmosphere (herein referred to as the oxidizing atmosphere) was used as a balance between slowing the oxidation rate by reducing the oxygen partial pressure, and inducing pitting. Ar-O₂ mixtures were used in order to avoid any complications due to nitride formation (a concern in TiAl which was exposed to the same atmospheres). In practice this atmosphere resulted in oxidation rates and oxide scales comparable to the results reported in the literature for exposures in "air". Pitting experiments were conducted in an atmosphere containing 50 ppm oxygen in HP Ar, at a temperature of 760° C. Additional oxidation experiments at 1000° C were conducted in this atmosphere for comparison. In order to determine if any effects could be observed due solely to thermal treatment of the implanted specimens, annealing experiments were conducted in either HP Ar or a reducing atmosphere containing Ar- 4.62% H₂. Experiments were conducted for durations of 5 minutes to 15 hours. The relatively short duration of most of the experiments reflects the philosophy that if no significant effects are detected in the short term nothing is likely to be observed in longer exposures. Furthermore, longer term experiments are outside the scope of this experimental approach, as the thicker scales produced in long experiments are not amenable to analysis with SIMS or Auger.

Surface Analysis

The as-implanted surfaces were examined using XPS and Auger electron spectroscopies. Both techniques provide information regarding the ionization state of Al, however only XPS provides reasonably clear determination of the Nb state. The spatial

and depth resolution of AES is considerably better than XPS however, consequently XPS was primarily utilized to determine near-surface oxidation states, while AES was used to map the variation of oxidation states observed through the implanted zone of the specimens. Consequently in the following discussion, AES results are emphasized, and XPS data is presented where it helps clarify the data.

By convention Auger energies are referred to by a three letter notation which indicates the inner shell from which the first electron was ejected and the two outer shells from which the electron to fill the inner shell vacancy arrived, and the Auger electron was ejected, respectively. Historically for the best sensitivity Auger spectra were collected in differential mode, $dN(E)/d(E)$ vs E . This serves to clearly distinguish the peaks from the high background present in electron spectra. This technique is essential when searching for trace elements. In this case however we are more concerned with determining the oxidation state of bulk elements. It is therefore possible to present the most of the data as $N(E)/E$ vs E plots. Since in this technique only the principal peak is visible, the undifferentiated spectra make demonstration of energy shifts due to oxidation more obvious. The principal Al Auger peak is the KLL which is centered at 1393.2 eV (all energies are given for peaks measured in the $N(E)/E$ vs E mode, and are taken from ref. 64 unless otherwise noted.) There is also a prominent LMM (LVV) peak at 64 keV. This peak actually proved to be more useful due to its less complex structure. These peaks are both shifted down in energy when the data is collected from oxidized Al. The KLL peak shifts by 6.5-7.4 eV, while the LMM peak is reported to shift by as much as 17 eV (minimum in differential mode)⁶⁷. The most intense Nb Auger peak is the MNN which

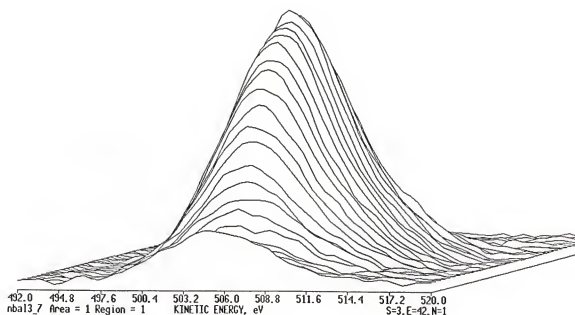


Figure 4-6 A: Auger spectra obtained from a depth profile of an as-implanted specimen of NbAl₃. This figure is a montage of oxygen KLL peaks gathered during a depth profile through the implanted region of a specimen of NbAl₃ implanted with $1 \times 10^{18} {}^{18}\text{O}$ ions/cm². The first two spectra from the surface have been removed for clarity. It is not possible to put an accurate depth scale on this data however the total depth profile is approximately 1 micron. The intensity of the peaks represent the variation in oxygen concentration through the implanted layer.

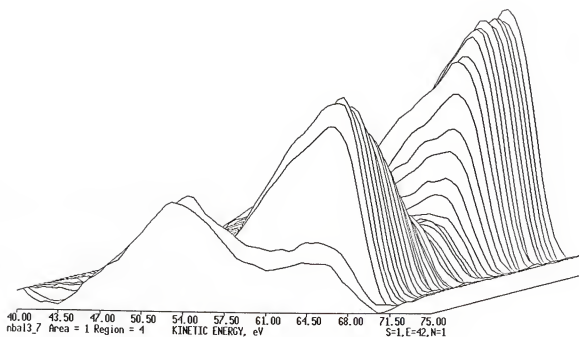


Figure 4-6 B: Auger spectra obtained from a depth profile of an as-implanted specimen of NbAl_3 . This figure is a montage of aluminum LVV peaks gathered during a depth profile through the implanted region of a specimen of NbAl_3 implanted with $1 \times 10^{18} \text{ }^{18}\text{O}$ ions/cm². In this case the surface peaks corresponding to the native oxide film are visible. In the implanted region (the valley marked) the majority of the signal once again shifts to the lower energy peak which demonstrates that the implanted oxygen has formed aluminum oxide.

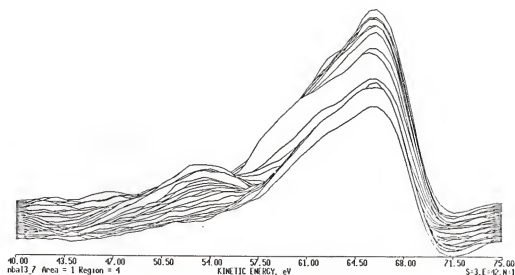


Figure 4-6 C: Auger spectra obtained from a depth profile of an as-implanted specimen of NbAl_3 . This figure is a montage of aluminum LVV peaks gathered during a depth profile through the implanted region of a specimen of NbAl_3 implanted with $1 \times 10^{18} \text{O ions/cm}^2$. This is a different view of the same data shown in 4-6 B. In this case the surface peaks corresponding to the native oxide have been removed. The lower energy peaks corresponding to the oxide formed by the implanted oxygen are indicated.

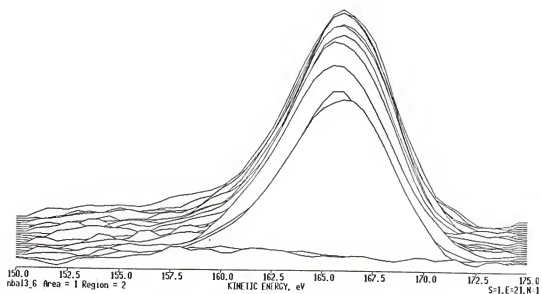


Figure 4-6 D: Auger spectra obtained from a depth profile of an as-implanted specimen of NbAl_3 . This figure is a montage of niobium MNN peaks gathered during a depth profile through the implanted region of a specimen of NbAl_3 implanted with $1 \times 10^{18} \text{ } ^{18}\text{O}$ ions/ cm^2 . Unlike the aluminum profiles, no shift in energy is observed for the Nb peaks in the implanted region. At the surface note that the Nb intensity is near zero, showing that the native oxide does not contain Nb, as confirmed by XPS.

occurs at 167 eV (differential mode). The KLL peak at 1944 eV is at very low intensity and was consequently not used in this study. The oxygen KLL peak was observed to occur centered at 503.5 eV in this study.

In figures 4-6 A-D are shown Auger spectra collected from a specimen of NbAl₃ implanted with 1×10^{18} ¹⁸O ions/cm² at 164 keV. These figures show a montage of spectra obtained by sputtering the area of interest with Ar for 12 seconds, collecting spectra from each element, then sputtering further. The total sputter time in this case was 8 minutes. By presenting the data in this format the changes that occur in the spectra due to the presence of the implanted oxygen can be easily demonstrated. 4-6A shows the peak due to the implanted oxygen distribution. 4-6 B and C are two different views of the Al LMM peaks. In B surface peaks are present which are clearly aluminum oxide. Deeper into the specimen the peaks appear to be due only to metallic Al, but at the depth where the oxygen has been implanted the metal peak almost completely disappears and the oxide peak at 54 keV appears. This peak is visible more clearly in fig. 4-6 B wherein the surface peaks are not shown and the spectra are not skewed. The oxide peaks are lower intensity than the metal peaks because of a combination of reduced atomic density and reduced Similar features are observed in the Al KLL data. These spectra show clearly that the implanted oxygen does form aluminum oxide in the as-implanted specimens. Figure 4-6 D shows the montage of the Nb MNN spectra obtained from this same specimen. At the surface the peak intensity is somewhat reduced, but no significant shift is apparent. XPS of this same specimen revealed that at the surface was a layer of aluminum, apparently all in the oxide state, and no Nb. After a brief Ar sputter (estimated as 50 Å) a small Al metal

peak appeared as well as the Nb $3d_{3/2}$ - $3d_{5/2}$ doublet which corresponded to Nb metal. The peaks were asymmetrical however which indicates that a minor amount of an oxide, possibly NbO, was present. Obtaining clean XPS spectra from the NbAl₃ was complicated however by the impossibility of avoiding cracked areas of the surface, which could not be efficiently sputtered. The surface of oxygen implanted pure Nb metal yielded a spectrum which corresponds to Nb₂O₅. This spectrum is clearly distinguished from Nb metal by a shift of 5eV. Unfortunately the depth resolution of the available XPS system does not allow sputtering to the depth of the implanted layer with any confidence. However it is clear that the near surface region contains a mixture of aluminum oxide and unoxidized Nb. All of this data is summarized in figure 4-7 which shows a depth profile of the same oxygen implanted NbAl₃ specimen. This spectrum was obtained using a three-point acquisition mode, wherein only three channels are used to collect data under each peak, one for the centroid and two for the background. This technique allows more rapid data collection, which tends to reduce noise in the profile, however all the fine details of the individual peaks are lost. In this profile the peak labeled Al2 is the aluminum oxide peak, and that labeled Al4 is the corresponding metal peak. Note that under the peak of the implanted profile the aluminum metal peak is reduced to background, while that of the oxide reaches the same level as the surface signal, which has been shown using XPS to be due entirely to aluminum oxide. The decrease in Nb signal intensity under the implanted peak is attributed to the local reduction in Nb number density due to the presence of the implanted oxygen.

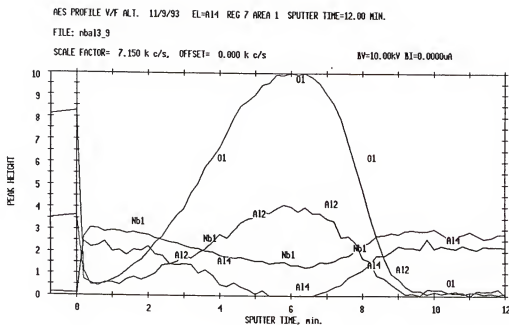


Figure 4-7. Auger depth profile measured from an as-implanted specimen of NbAl_3 . The implanted oxygen distribution is clearly visible. The profile labeled Al2 is the intensity of the Al LMM oxide peak centered at (52-54) eV, while that labeled Al4 is the corresponding metal peak at 64 eV.

Secondary Ion Mass Spectrometry

Introduction

SIMS analysis was performed in all cases using a Cs⁺ primary ion beam. Negative ions were collected for all species. The principal secondary ions of interest were ¹⁶O₂⁻, ¹⁸O₂⁻, ²⁷Al⁻, and Nb⁻. The dimer ions were collected to reduce interferences and because the monomer signal tended in some cases to saturate the detection system. In addition AlO⁻ and NbO⁻ profiles were collected in order to provide corollary information. The superposition of all of these profiles on a single plot is illegible, so in all of the data presented below, the profiles are limited to those species which show the important results most clearly. In most cases two plots of data from the same sputter profile are used for clarity.

Raw SIMS data is collected as intensity of counts at a given mass as a function of time. At a single primary ion intensity, the detected intensity for a particular element varies as the concentration of the element in the substrate, and the chemical bonding of the element or the matrix of which it is a component. The intensities of different elements vary depending on their ionization and elastic scattering cross-sections which vary with primary ion energy. In most cases negative SIMS depth profiles were collected. Negative profiles maximize the sensitivity for oxygen isotopes, although some metal ion sensitivity is lost. Since the metal ions in this case are from the matrix elements, sensitivity was not an issue. Singly charged ions were collected in all cases except for the oxygen isotopes, for which the singly charged intensity was too high.

The objective of the SIMS analysis in this study was to determine the location of the implanted layer and observe what changes it underwent due to high temperature oxidation, both by direct measurement of implanted specimens and by comparison to non-implanted specimens. Since the ability to compare spectra was so important, every effort was made to minimize artifacts due to instrumental variations. Insofar as possible the same instrumental settings were used for all of the specimens. For comparisons of non-implanted versus implanted specimens, different areas of the same coupon were used. The analyses of these different areas were conducted during the same session on the instrument. All of the specimens were metallographically polished prior to the implantation in order to minimize effects due to surface topography. (As was discussed above, the oxygen implantation did not result in significant surface topography.) In most cases spectra were collected repeatedly from similar areas, especially if any unusual effects were observed. Consequently the significant differences observed between specimens are due to differences in surface treatment and thermal history, and may not be attributed to instrumental variation or, in general, to specimen inhomogeneity. The significance of the differences which are observed requires some background in interpretation of SIMS spectra however. Of particular importance are the effects of interferences, surfaces, interfaces, and matrix effects.

Interferences in SIMS data can occur from the presence of ions at the same mass as the ion of interest but due to a different species. The most important interference in this study would be due to the superposition of $^{18}\text{O}^+$ and H_2O^+ . Only negative ions were collected for most of the profiles. Since the intensity of H_2O^- ion is negligible, this

potential interference is not a problem. Another possible interference is due to C^{12}_2 and O^{18}_2 , however the concentration of carbon in the specimens is not high enough for this to be a problem. In general there are no significant mass interferences which occur in the systems examined in this study.

At the surface sputtering yields are at a minimum due to the presence of a native oxide film. The surface may act as an insulator, which becomes charged and tends to repel further primary ions. This effect may be very noticeable in some specimens, and results in a surface sputtering rate that is much slower than in the bulk. Oxidized specimens show especially noticeable surface charging effects, in addition to broadening of the elemental profiles caused by surface topography. Since the sputtering yields (defined as the number of secondary ions produced per primary ion) of different species vary there is also a transient effect observed at the surface as the rate of sputtering of individual species is not yet at equilibrium. This results in a slope in the elemental profiles near the surface in the absence of any other effects. If the yield for one element is very different from that of the matrix, the apparent concentration can change significantly, due to the preferential loss of one species. The sputtering yields for Nb and Al are fairly close together, they are reported as 1.3 and 1 respectively for 500 eV Ar ions.⁶⁸ For Cs ions the yields may be closer still, as no significant changes in relative signal were observed for profiles into the non-implanted NbAl₃ matrix.

Artifacts can occur in SIMS spectra due to changes in sputtering rate or yield at particular points within the specimen. Interfaces are the most common sources of artifacts. At an interface the yield of the substrate species may change by orders of magnitude. The

width of the interface in the SIMS profile will appear to be greater than it is in the substrate.⁶⁹ Interfaces in the specimens examined in this study are in general not sharp, due to the nearly Gaussian profiles of the implanted species, and the profiles of oxygen diffused into the specimens during oxidation. Therefore interface effects result in some cases in broad local maxima or minima in the elemental concentration profiles. Precise determination of interface depth is therefore not usually possible in this study, however the effects due to interfaces serve to mark the areas in which structures due to ion implantation have been precipitated.

Matrix effects are changes in ion yield due to the local environment of the ion of interest. The presence of reactive species within the layer being sputtered tends to increase the yield of metal ions. This effect is especially evident for oxygen, and is observed in all of the profiles. Changes in bonding also changes the ion yield. The presence of an oxide layer for example, may result in a local maximum or minimum in the metal ion yield.

All of the above effects complicate analysis of SIMS data. Since the intensity of a single ion is not in general a linear function of concentration, and the intensities of different ions may not be simply related, it is not possible to put a meaningful vertical axis on composite SIMS profiles in terms of concentration. Therefore the vertical axis in all of the profiles presented below is in arbitrary units of intensity. A good idea of the concentration of a given element at some point in the profile can be obtained by comparing its local intensity to its intensity in the matrix, which in all cases is the region on the right hand side of the plot where the elemental concentrations run parallel to each other. The horizontal axis is sputter time in minutes. This scale has been converted to depth in a few

cases by measuring the pits from which the data was collected.. Depth measurements were performed using a Dektak profilometer. Since the sputter rate may change with the composition of the matrix, there is a systematic error in the depth scale. The magnitude of this effect was estimated by sputtering craters for different lengths of time in some specimens. The variation between similar specimens is insignificant, but is very noticeable when comparing specimens which underwent very different treatments, such as annealed vs. oxidized. Depth scales are therefore given for comparison purposes, but must be regarded as imprecise.

As-Implanted NbAl₃

The as-implanted SIMS profile of a specimen of NbAl₃ implanted with 10^{18} ^{18}O ions/cm² is shown in fig. 4-8. A number of characteristic features are visible. Note that in contrast to the calculated profile of fig. 4-1, the oxygen profile is nearly flat over a range of about 1000 Å. This is more similar to the distribution of fig. 4-5, which was calculated assuming that the implanted oxygen formed alumina directly. This result indicates that the matrix is saturated with oxygen and may have formed a continuous oxide layer, as determined by Auger. In other words the appearance of this profile provides direct evidence that at a dose of 1×10^{18} ^{18}O ions/cm² that a continuous, nearly stoichiometric oxide layer is formed. The formation of a saturated layer over this range requires that some diffusion of oxygen and possibly of metal species, has occurred during the ion implantation. Otherwise it is expected that a narrower oxygen distribution, with a higher peak concentration would be reached. Essentially all of the aluminum in this layer has

been shown to be bound as aluminum oxide, based upon the Auger results discussed above. A local minimum in the Al concentration occurs, simultaneous with a maximum in the Nb. This could be due to a matrix effect, whereby the presence of the implanted layer enhances the emission of Nb ions while the Al ion intensity is reduced due to the Al being bound as oxide. This could also be the result of an actual local decrease in Al concentration, due to the lighter element being preferentially knocked off lattice sites and driven further into or out of the substrate by the incoming O ions. This mechanism is also consistent with the observed local increase in Nb ion intensity, as the relative concentration of Nb would increase as that of Al decreased. Fig 4-9 shows a profile from a specimen implanted at a dose of $2 \times 10^{17} \text{ }^{18}\text{O ions/cm}^2$. At this dose there is not sufficient implanted oxygen to form a continuous oxide layer. Both the Nb and Al intensities are enhanced under the implanted peak, with the enhancement for Nb more noticeable. The presence of the implanted layer is clearly responsible for the local increase in Nb signal. There is apparently a slight local minimum in Al intensity in this specimen as well, although overall the Al signal is above that of the matrix. Since there is a factor of five difference in the dose between these two specimens, the factor of two decrease in Al intensity under the peak in the higher dose specimen may be explained by preferential displacement of Al away from the region of maximum oxygen dose.

Annealed NbAl₃

Figures 4-10 through 4-13 show profiles obtained from a specimen of NbAl₃ annealed in Ar-4.62% H₂ at 1000° C for 30 minutes. The reducing gas mixture was chosen

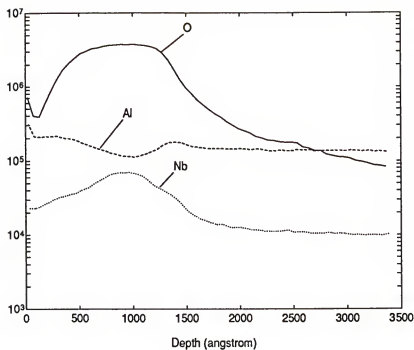


Figure 4-8. SIMS profile from a specimen of NbAl₃ as-implanted with 1×10^{18} ^{18}O ions/cm² at 160 keV. The horizontal axis in this case has been converted to depth by measuring the overall depth of the SIMS crater.

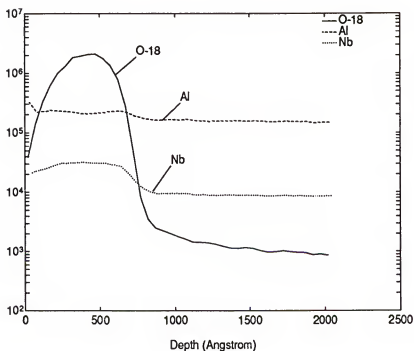


Figure 4-9. SIMS profile from a specimen of NbAl₃ as-implanted with 2×10^{17} ^{18}O ions/cm² at 100 keV.

since earlier experiments (conducted with specimens implanted at 2×10^{17} ions/cm²) in UHP Argon passed through a gettering furnace, had resulted in visible surface oxide layers. These profiles were collected from non-implanted (4-10 and 4-12) and oxygen implanted (4-11 and 4-13) regions of the same specimen. The objective of this experiment was to determine the effect of thermal treatment of an implanted specimen, in the absence of a moving oxidation front. Unfortunately this objective is complicated by the fact that it is almost impossible to obtain an atmosphere sufficiently free of oxygen to prevent any oxidation of an aluminum alloy at 1000°C, even in what should be a reducing environment. The technique used for this experiment was to lower the specimen into a tube furnace, open at the top, through which the annealing gas had been flowing for several hours. The condition of the atmosphere was judged based on the appearance of blank specimens of NbAl₃ which were exposed prior to the implanted specimen. When the blank specimens did not appear to be oxidized after 30 minutes the atmosphere was considered ready for the experiment. After the experiment the implanted specimen appeared to have reacted however. Overall the surface of the specimen still appeared to be metallic, however in the implanted region some surface material loss appeared to have occurred. Small flakes of metal apparently had spalled off of the surface, near the edges of the pre-existing cracks. The steps produced by this phenomenon were so shallow that was not possible to image them in the SEM, however they were visible optically and these regions were avoided when measuring the SIMS profiles. This phenomenon suggests that some reaction between H₂ and the implanted oxygen occurred, as it was not observed in the non-implanted areas. The presence of surface damage near the pre-existing cracks

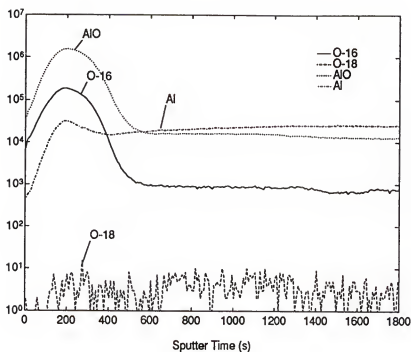


Figure 4-10.
SIMS depth
profiles of
aluminum species
measured from the
non-implanted
region of a
specimen of
 $NbAl_3$ annealed
for 30 minutes in
 $Ar-4.62\% H_2$

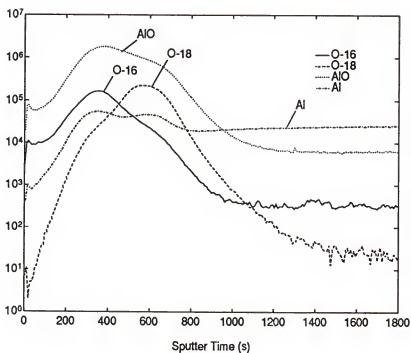


Figure 4-11.
SIMS depth
profiles of
aluminum species
measured from the
oxygen-implanted
region of a
specimen of
 $NbAl_3$ annealed
for 30 minutes in
 $Ar-4.62\% H_2$.

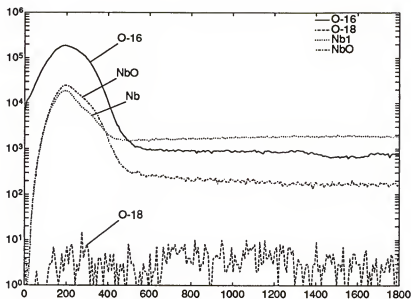
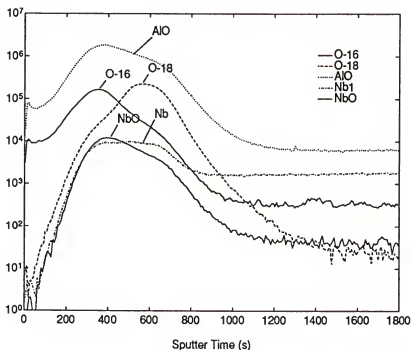


Figure 4-12. SIMS depth profiles of aluminum species measured from the non-implanted region of a specimen of NbAl₃ annealed for 30 minutes in Ar-4.62% H₂.



4-13. SIMS depth profiles of niobium species measured from the oxygen-implanted region of a specimen of NbAl₃ annealed for 30 minutes in Ar-4.62% H₂. The AlO spectrum is included for reference in this and subsequent figures.

implies that perhaps hydrogen penetration laterally into the surface from the cracks reacted with the implanted layer with a resulting stress that caused local spallation. Nonetheless since there was ample undamaged surface remaining, this specimen was judged to be usable.

Some oxidation did occur in this experiment, as can be deduced from the ^{16}O profiles present in all of the figures. Although this was not a completely inert environment however, the results of this experiment are very interesting. The depth of oxygen penetration appears to be slightly greater in the implanted specimen. The implanted oxygen distribution appears to have broadened and the peak is now located deeper into the specimen. It is clear that in both regions an alumina layer has formed at the surface, as shown by the Al and AlO profiles continuing smoothly to the surface while the Nb and NbO profiles fall by four orders of magnitude. This is consistent with the known oxidation kinetics of NbAl_3 . In the implanted specimen the surface oxide is thicker, which suggests that some enhanced Al cation diffusion has occurred in the near surface region. Since in the implanted layer most of the aluminum present has been oxidized, there is a gradient in Al metal activity which could result in short range Al diffusion into the implanted layer. Short range diffusion would be accelerated by the high defect concentration in the region near the peak of the implanted distribution. This is further supported by the local maxima in the aluminum intensity, which is in contrast to the minimum observed in the as-implanted specimen discussed above. In fig. 4-9 note that a small surface peak occurs in all of the profiles which does not appear in fig. 4-8. This suggests that there is a difference

in the surface structure of the implanted specimens, which is not limited to the area under the implanted oxygen peak.

Contrasting the NbO and Nb profiles in fig. 4-13, note that the NbO profile drops below that of the Nb, and parallels the drop in the ^{16}O profile. This suggests that niobium oxide is formed by atmospheric oxygen, even in the region under the implanted peak. The AlO profile shows a similar effect. The asymmetrical decrease in these profiles is due to the fraction of Al and Nb which are bound to ^{18}O , which does not contribute to the $\text{Al}^{27}\text{O}^{16}$ or the $\text{Nb}^{84}\text{O}^{16}$ profiles. Finally note that although oxygen penetration and cation diffusion have occurred in the implanted specimen, the depth of the ^{16}O penetration is no deeper than the tail of the implanted ^{18}O distribution.

Oxidized NbAl₃

A series of oxidation experiments were conducted with NbAl₃ in two different environments. "Normal" oxidation experiments were conducted at 1000°C in Ar-O₂ for periods of 30 minutes to 15 hours. "Pesting" experiments were conducted at 760°C in Ar-50 ppm O₂ for up to 10 hours. SIMS analysis of both the oxidation and the pesting experiments are discussed below.

Figures 4-14 through 4-17 show SIMS profiles measured from a specimen of NbAl₃ implanted with oxygen and subsequently oxidized in Ar-0.1% O₂ at 1000° C for 30 minutes. For clarity the profiles have been separated to show the data for Al and Nb species separately. Figs. 4-14 and 4-16 are profiles obtained from the same point in a non-implanted area of the specimen, while 4-15 and 4-17 are the profiles from the

implanted surface. Upon a cursory examination of the implanted profiles it is immediately obvious that a distinct change in oxidation mechanism has occurred. There are three distinct peaks in the all of the profiles from the implanted region except for the implanted ^{18}O , for which there are two peaks. In contrast, over a similar depth in the non-implanted region there is only a single peak in the AIO distribution which is paralleled by the Al and ^{16}O distributions.

Since it was already shown in the annealed specimen that ^{16}O penetrates to the depth of the implanted layer in 30 minutes, the shape of these implanted profiles can not be attributed to regions which are not oxidized. The most plausible explanation is that these peaks are due to interface effects and that a multi layered structure has been formed in the surface oxide due to the presence of the implanted oxygen. The first peak near the surface is due to enhanced emission from the surface which formed a surface layer which apparently sputters more easily than the non-implanted surface. Note that at the surface the ^{18}O signal is at background levels, indicating that the surface consists of atoms which did not fall within the implanted layer. The second and third peaks are thought to indicate the borders of an oxide layer that has formed in the region of the implanted oxygen distribution. This layer is distinct from that formed on the surface because it contains a unique distribution of defects caused by the implantation and, in effect, frozen in by the combination of the implanted oxygen and the additional oxygen which diffused in from the surface. The near surface peak of this region may be due to a small amount of diffusion of implanted ^{18}O toward the surface, however it is more likely that this is merely an enhancement due to the interface effect. This explanation is consistent with the effects

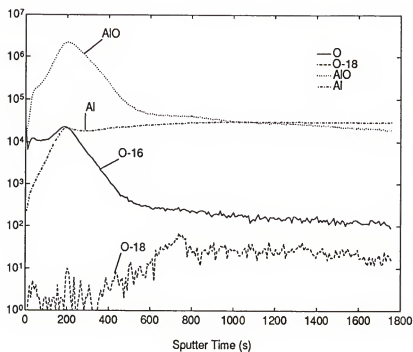


Figure 4-14. SIMS depth profiles of aluminum and oxygen species measured from the non-implanted region of a specimen of $NbAl_3$ oxidized for 30 minutes at $1000^\circ C$.

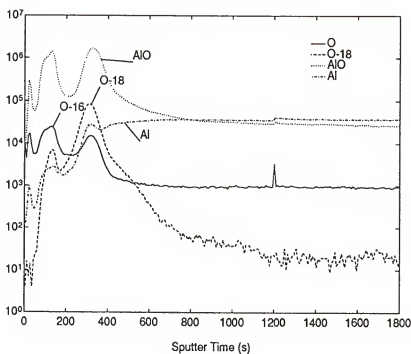


Figure 4-15. SIMS depth profiles of aluminum and oxygen species measured from the oxygen implanted region of a specimen of $NbAl_3$ oxidized for 30 minutes at $1000^\circ C$.

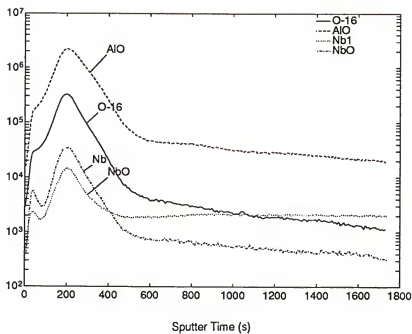


Figure 4-16. SIMS depth profiles of niobium and oxygen species measured from the non-implanted region of a specimen of NbAl_3 oxidized for 30 minutes at 1000°C .

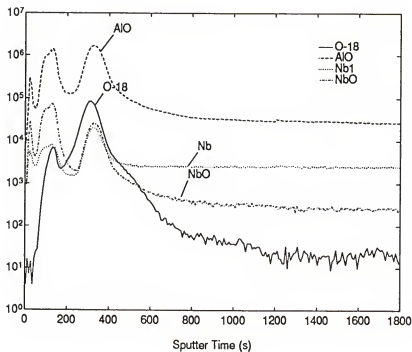


Figure 4-17. SIMS depth profiles of niobium and oxygen species measured from the oxygen implanted region of a specimen of NbAl_3 oxidized for 30 minutes at 1000°C .

observed in the implanted specimens as well as fitting the likely structure of the implanted layer, which would consist of a defective aluminum oxide supersaturated with dissolved niobium. Such a structure would favor cation diffusion, consistent with the formation of a surface oxide containing metal ions which diffused out of or through the implanted layer, while it is clear that oxygen does not penetrate beyond the tail of the implanted oxygen distribution.

Figures 4-18 through 4-21 show profiles measured from non-implanted and oxygen implanted regions of a specimen oxidized at 1000° C in Ar-0.1% O₂ for 15 hours. Once again the profiles have been separated in order to more clearly show the effects of implantation on the Nb and Al distributions. These profiles are interpreted as a maturing of the structures observed in the specimen discussed above which was oxidized for 30 minutes. The most striking difference between the profiles is the surface peaks observed in the implanted regions. This structure does not occur in the non-implanted regions, and is clearly the result of the oxygen implantation, although not directly associated with the implanted oxygen peak. The implanted oxygen peak has broadened from that observed at 30 minutes and the maximum has dropped by approximately a factor of two. Apparently some diffusion has occurred in the implanted species, (or the peak is broadened due to slower sputtering) however the AlO and ¹⁶O distributions still follow the tail of the ¹⁸O distribution. The near surface peak appears to be due to outward cation diffusion through the implanted region. This peak has now incorporated both the surface peak and the middle peak observed in the specimen oxidized for 30 minutes. This phenomenon would apparently suggest that this peak represents epitaxial growth of the oxide region observed

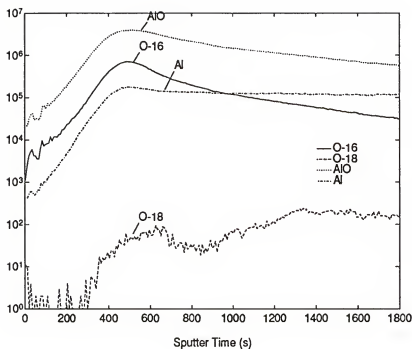


Figure 4-18.
SIMS depth
profiles of
aluminum and
oxygen species
measured from the
non-implanted
region of a
specimen of
NbAl₃ oxidized for
15 minutes..

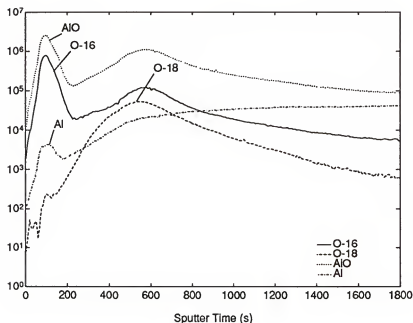


Figure 4-19.
SIMS depth
profiles of
aluminum and
oxygen species
measured from the
oxygen implanted
region of a
specimen of
NbAl₃ oxidized for
15 hours..

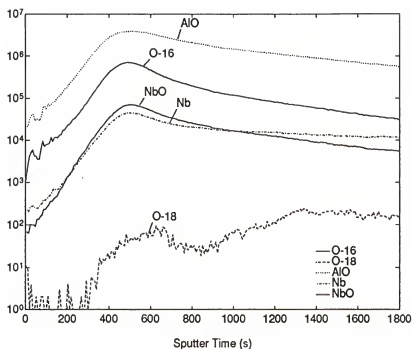


Figure 4-20.
SIMS depth
profiles of
niobium and
oxygen species
measured from the
non-implanted
region of a
specimen of
 NbAl_3 oxidized for
15 hours..

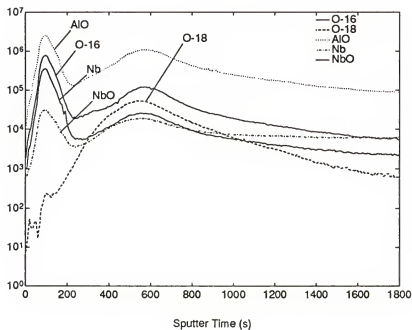


Figure 4-21.
SIMS depth
profiles of
niobium and
oxygen species
measured from the
oxygen implanted
region of a
specimen of
 NbAl_3 oxidized for
15 hours..



Figure 4-22. Macrograph of the specimen of NbAl₃ implanted with 1×10^{18} O ions/cm² and subsequently oxidized for 15 hours at 1000° C (left) and another similar specimen exposed in Ar-500 ppm O₂ at 760° C for 4.5 hours (right). In both specimens the implanted region is within the semicircular area visible to the right side of the photo below the suspension holes.

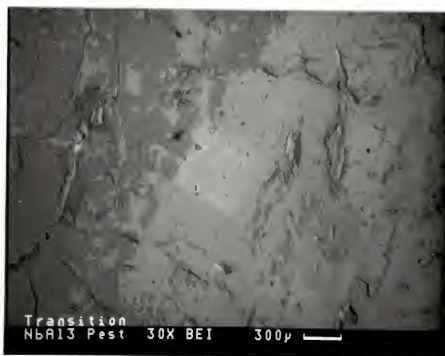


Figure 4-23. SEM micrograph of the surface of a specimen of NbAl₃ implanted with 1×10^{18} ¹⁸O ions/cm² and subsequently oxidized for 4.5 hours at 760° C in Ar-50 ppm O₂. The transition region is in the center of the micrograph, with non-implanted and implanted regions to the left and right respectively. The square area at the center of the photo is a SIMS crater in the transition region from which the data for figures 4-28 and 4-29 was collected.

after 30 minutes, since the peak is attributed to the crystal structure and composition of the layer as distinguished from that formed on the non-implanted region.

The oxide on this specimen appeared to be lighter colored and more uniform on the implanted region. A macrograph of this specimen is shown in fig. 4-22. Clearly the presence of the implanted layer does result in the formation of an oxide layer which causes an apparent change in the high temperature oxidation mechanism. The most serious oxidation problem associated with NbAl_3 (as well as many other line compounds) is "pesting" however. Consequently a series of experiments were conducted in order to determine if the pesting phenomenon could be affected by the presence of an implanted oxygen layer.

Influence of Ion Implanted Oxygen on the Mechanism of Pest in NbAl_3

There are several theories regarding the cause of the pesting phenomenon observed in NbAl_3 and other intermetallic compounds. These are discussed in the literature review. For the present discussion it may be recalled that the phenomenon involves disintegration of polycrystalline specimens at intermediate temperatures and reduced oxygen activities. Proposed mechanisms for the pest in NbAl_3 involve either precipitation of alumina at grain boundaries resulting in a crack-opening wedge¹⁰ or, more recently, the internal precipitation of Nb_2Al at grain boundaries due to loss of Al to the surface.¹¹ These mechanisms are distinctly different in that they propose that the mechanism is due to oxygen transport inward or Al cation transport to the surface. Since the presence of the

implanted layer has been shown to favor outward cation transport over anion transport, it seems logical that it might affect the mechanism involved in pesting as well.

Since the specimens used in this study were cut from an as-cast ingot, they contained very large grains and extensive porosity. Consequently these specimens are expected to be particularly susceptible to pesting. The ion-beam implantation process is limited to line of sight, therefore the cracks and porosity must prevent parts of the surface from being implanted. Furthermore none of the specimens were implanted over the entire surface. Therefore it was expected from the outset that these specimens would exhibit pest, but hopefully a significant difference between implanted and non-implanted specimens could be observed. This did in fact turn out to be the case.

Pesting experiments were conducted in an atmosphere of 50 ppm O_2 in Argon at 760° C. Four experiments were conducted. All of the specimens started to exhibit disintegration after 4-6 hours of exposure. The implanted surfaces however proved to be significantly resistant to disintegration, even after the rest of the sample had crumbled. The implanted areas of all of the specimens were colored dark green or blue-green after the exposure, while the non-implanted areas had turned dark gray or black, and had largely disintegrated.

The first specimen to be tested disintegrated and fell off of the hangdown to the bottom of the furnace after approximately 6.5 hours. The suspension hole on this sample had been drilled through the non-implanted region. The non-implanted area of the specimen had completely crumbled into a coarse powder, resulting in the sample falling. Upon retrieving the remains of the specimen from the furnace however, the implanted area

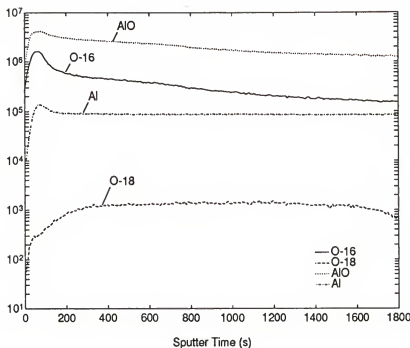


Figure 4-24. SIMS depth profiles of aluminum and oxygen species measured from the non-implanted region of a specimen of NbAl_3 exposed for 4.5 hours at 760°C in Ar-50 ppm O_2 .

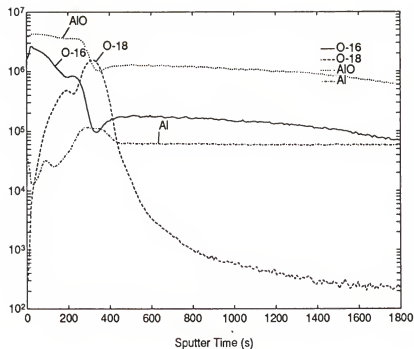


Figure 4-25. SIMS depth profiles of niobium and oxygen species measured from the oxygen implanted region of a specimen of NbAl_3 exposed for 4.5 hours at 760°C in Ar-50 ppm O_2 .

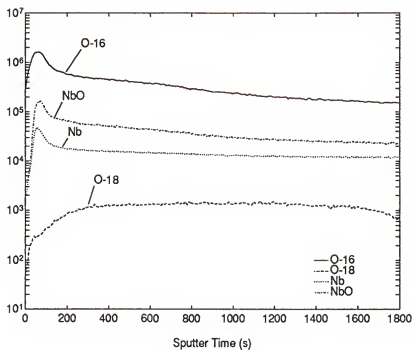


Figure 4-26. SIMS depth profiles of niobium and oxygen species measured from the non-implanted region of a specimen of NbAl_3 exposed for 4.5 hours at 760°C in Ar-50 ppm O_2 .

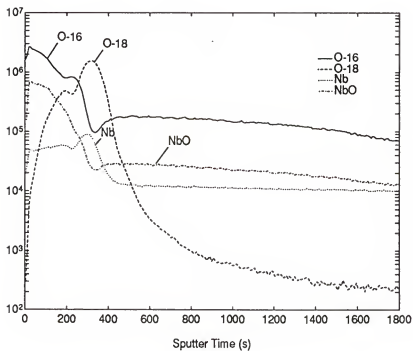


Figure 4-27. SIMS depth profiles of niobium and oxygen species measured from the oxygen implanted region of a specimen of NbAl_3 exposed for 4.5 hours at 760°C in Ar-50 ppm O_2 .

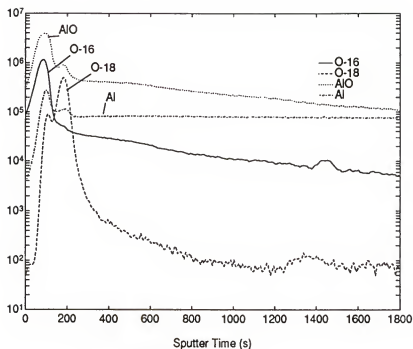


Figure 4-28. SIMS depth profiles of aluminum and oxygen species measured from the transition region of a specimen of $NbAl_3$ exposed for 4.5 hours at 760°C in Ar-50 ppm O_2 .

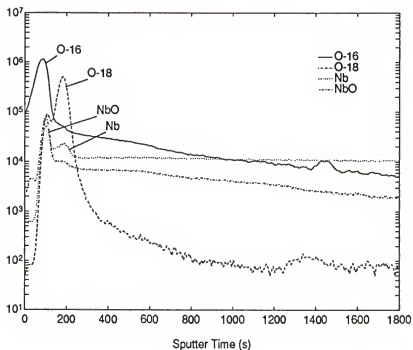


Figure 4-29. SIMS depth profiles of niobium and oxygen species measured from the transition region of a specimen of $NbAl_3$ exposed for 4.5 hours at 760°C in Ar-50 ppm O_2 .

of the specimen was found to be completely intact. This was in spite of the fact that the back side of this specimen was not implanted, and was beginning to spall. This experiment was repeated immediately however the microbalance was closely monitored and the specimen was removed when the first weight loss was observed. Once again the implanted area was colored dark green, while the non-implanted area was mottled grey/black. A micrograph of this specimen is shown in fig. 4-23 This specimen was used also for SIMS analysis.

Figures 4-24 through 4-29 are show SIMS profiles taken from three different areas of the peeting specimen. 4-24 and 4-25 emphasize the Al distribution measured in non-implanted and implanted areas, respectively, while 4-26 and 4-27 show profiles of the Nb species. Figures 4-28 and 4-29 show the Al and Nb distributions measured in an area at the edge of the implanted region. This region at the edge of the implanted target region is referred to herein as the transition region between the implanted and non-implanted areas of the surface.

A dramatic difference is evident between the non-implanted and implanted profiles. The Al and Nb profiles both exhibit local maxima at the same location, once again showing the metal ion enhancement under the implanted oxygen curve seen in the annealed and oxidized specimens. The AlO, NbO and ^{16}O profiles all exhibit minima at the location of the maximum in the implanted ^{18}O profile. Comparison with the non-implanted profiles shows that the AlO, NbO and ^{16}O levels in the matrix beyond the implanted peak are a factor of five lower than in the non-implanted specimen. After the clearly defined drop at the position of the implantation maximum, these species apparently are at

background levels. This shows that the pesting resistance observed in the oxygen implanted areas of the specimen may be attributed to a virtual halt to oxygen anion diffusion into the specimen surface. Furthermore this strongly suggests that the pesting phenomenon in NbAl_3 is dependent on oxygen dissolution rather than cation diffusion and resulting phase transformation, as proposed by Topylgo and Grabke.¹¹ Of course the limited solubility range and non-existent plasticity of NbAl_3 must play a role in the pesting phenomenon, but the dominant mechanism appears to be oxygen dissolution and transport down grain boundaries.

Figures 4-28 and 4-29 illustrate a further interesting phenomenon. As previously stated, these profiles were measured from the transition region of the surface, where the implanted oxygen dose is much lower (by a factor of 2-5 according to Dr. S.P. Withrow of SMAC-ORNL) than in the main implanted area of the surface. The implanted peak in this area appears to be narrower than in the main implanted area, and the ^{18}O peak height is lower by roughly a factor of 2. Nonetheless the same effect of reduced oxygen penetration is observed in this area as in the rest of the implanted surface. As previously mentioned, even at the highest dose used in this study, it is impossible to completely saturate an area with oxygen. Consequently the effectiveness of this implantation technique in forming a protective oxide layer may be thought of as depending on unsaturated bonds in the implanted region being quickly filled by oxygen diffusing in from the environment, resulting in a unique oxide structure which is resistant to further anion transport. The results observed here indicate that this objective may be achieved with a layer implanted with an oxygen dose a factor of 2-5 lower than that used in most of this

study. In fact this conclusion had been suggested by earlier results using specimens implanted at $1\text{-}2\times 10^{17}$ ions/cm².⁷¹ However the higher dose was utilized in order to optimize the stability of the implanted surface under all conditions, as well as to maximize the signal to noise ratio of the implanted species for Auger and SIMS analysis.⁷²

The results of these experiments were sufficiently positive that two follow up experiments were conducted using specimens of NbAl₃ which were implanted on approximately two thirds of both sides. The implanted areas were positioned opposite to each other in order to maximize the protection of the substrate between the implanted regions. These specimens did not exhibit any particular improvement in pesting resistance over that discussed above however. This result is attributed to the same difficulties. The presence of pre-existing cracks and large grain boundaries, as well as the impossibility of implanting the edges of the specimen, makes it impossible to effectively protect the entire surface. The pesting reaction therefore proceeds in the non-implanted regions and eventually undermines the implanted surfaces. Although these surfaces did survive intact, most of the underlying specimen disintegrated anyway. It would be extremely interesting to try this experiment on specimens of high density fine grained NbAl₃ (produced by powder processing) and on single crystal material. These experiments are not within the scope of the present work however.

X-Ray Diffraction

X-ray diffraction was used in an attempt to determine the crystal structure of the implanted oxide layer. A Phillips APD 3720 powder diffraction system was used.

Continuous scans from $10-90^\circ 2\theta$ were investigated as well as very slow step scans over likely angles in which peaks from non-equilibrium oxide phases would be detected. In as-implanted and annealed specimens, only peaks corresponding to NbAl_3 were detected. In oxidized specimens the only additional peaks were due to alumina. Consequently no unusual crystallography can be attributed to the implanted surface based on the available evidence.

Summary of Results of Implantation of Oxygen in NbAl_3

The objective of this investigation into oxidation of aluminide intermetallic compounds was to determine if an improvement in oxidation resistance could be achieved using high dose ion-implantation of oxygen. Specifically this objective relied on determining if oxides were formed by the implantation process, and whether the resulting oxide layer could be shown to reduce the thickness of the oxide scale grown during high temperature oxidation. The implanted layer was shown to result in a layer in which practically all of the aluminum was oxidized (using Auger spectroscopy). Neither the as-implanted, annealed, nor the oxidized specimens produced X-ray diffraction patterns with peaks attributable to any phases other than alumina or NbAl_3 . This suggests that while the morphology of the implanted layer may be unusual, the crystallography is that of the equilibrium phases. SIMS analysis of the surfaces of all of the specimens showed that under all of the conditions tested that the implantation process resulted in a decrease in subsequent oxygen penetration into the surface of the specimen. This shows that the principal of the process is valid and that improvement in oxidation resistance can be

achieved using preoxidation with ion implantation. Finally it has been demonstrated that the pesting phenomenon in NbAl_3 is dependent on the penetration of oxygen through the outer surface. This lends support to the "crack opening wedge" hypothesis of Steinhorst and Grabke¹⁰ but tends to contradict the Al loss/phase transformation hypothesis of Topylgo and Grabke.¹² Further research into the mechanism of pest in NbAl_3 is apparently required.

CHAPTER 5

OXYGEN IMPLANTED TiAl

Ion Implantation

The same system was used for implanting TiAl as for the NbAl₃ discussed in the previous chapter. In the interest of clarity the same discussion of implant parameters is repeated here. As a practical limit the maximum dose used for all of the implants in this study was 1×10^{18} ions/cm². This limit was dictated by the maximum current of ¹⁸O available in the ion beam using the Varian Extrion 200 kV implanter at SMAC-ORNL. In the initial experiments it took approximately three hours to implant an area of 10 cm². As this research progressed improvements in the implanter and further experience with ¹⁸O beams shortened the time required to reach the maximum dose to approximately 90 minutes. The objective of the implants was to obtain a sufficient concentration of oxygen in the implanted specimen that a continuous layer of M₂O₃ stoichiometry could be formed. It was assumed that sufficient oxygen is implanted to combine with all of the available aluminum if a peak concentration of 0.6 times the Al concentration in the target alloy is achieved. Although this clearly results in an implanted region which contains insufficient oxygen to combine with all of the available metal atoms, in order for a layer to form which consists of continuous Al₂O₃ additional aluminum atoms must diffuse into the implanted layer and the other component, Ti in this case, which remains in the implanted layer must

either be dissolved in the oxide or diffuse out to the surface to form a separate oxide layer.

Modeling using the PROFILE code indicated that at a dose of 1×10^{18} ^{18}O ions/cm² and an accelerating energy of 170 keV a peak concentration of 49.2 % oxygen could be reached with the implanted layer extending from near the surface to a depth of 350 nm. The calculated distribution is shown in figure 5-1. Figure 5-2 shows a calculated profile for the same dose in which it is assumed that the implanted oxygen forms alumina. The oxygen distribution in this case is somewhat broader and extends to a depth closer to 400 nm. The predicted surface recession in this case is 586 Å vs 901 Å in the case where no compound formation is assumed. In either case the calculated profiles are based on oversimplifications of the actual process involved and are therefore taken to be semi-quantitative. The retained dose (near 100%) is probably correct due to the depth of implantation, and the actual peak depth is expected to lie near the calculated depth. The distribution of oxygen is however expected to be further modified by the competition of Ti with Al for binding to the implanted oxygen. Due to the very similar oxygen affinities of Al and Ti it is unlikely that either metal will capture all of the oxygen in the as-implanted layer. Although Al_2O_3 is very stable under irradiation, rutile has been formed in high-dose oxygen implantation of pure Ti metal.⁴⁸ Therefore neither metal seems to be more likely to form a stoichiometric oxide. The lower mass of Al may result in it being displaced from the implanted region more easily than Ti, resulting in Ti enrichment under the implanted peak. Assuming that the concentration of O does reach 49% under the peak and that the number density of Al and Ti remain in the ratio of 1:1 then the metal in the implanted layer

will be in an oxide layer of the approximate stoichiometry AlTiO_2 or AlOTiO . This is not a stable structure and is expected to reorder when exposed at high temperature.

Two specimens of TiAl were implanted with Ne in an attempt to produce a level of radiation damage in the specimen equivalent to the oxygen implants without any potential for compound formation. The calculated profile for implantation of ^{20}Ne at 170 keV and a fluence of 1×10^{18} ^{20}Ne ions/cm² is shown in figure 5-3. This profile is very similar to figure 5-1 except that the peak depth is slightly less due to the greater mass of Ne.

Auger Electron Spectroscopy

The as-implanted surfaces were examined using Auger spectroscopy in order to determine the depth distribution and oxidation state of the Al and Ti in the implanted region. XPS was used for cross reference however Al and Ti oxidation states may be identified using Auger or XPS peak shift and changes in peak shape, both in the pure metals^{64,73,74} and in TiAl^{75,76,77}. The most significant peak shifts due to oxidation occur in transitions involving the valence band electrons. In pure Al the LVV peak at 64 eV shifts downward in energy by as much as 17 eV⁶⁴. In TiAl Shanabarger⁷⁶ observed this peak at 66.8 eV (differential mode) on the pure metal. After exposure to oxygen this peak appeared as a doublet with minima at 40.8 and 56.4 eV. In the same reference the Ti MVV triplet was reported to shift only slightly, from 386.7, 417.9, 450.7 eV to 385.0, 417.9, 451.1 eV. The width of the differential peaks in the Ti MVV spectrum increase in the oxide state. Most significantly for this investigation the relative magnitude of the principal peaks changes, with the maximum intensity at the lower energy peak surpassing

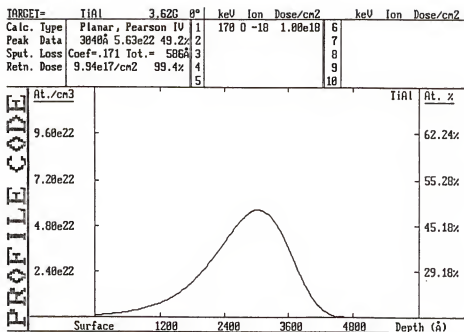


Figure 5-1. The oxygen distribution obtained using the PROFILE code for implantation of 1×10^{18} ^{18}O ions/cm² at 170 keV into a TiAl target. The maximum oxygen concentration predicted is 49.2%.

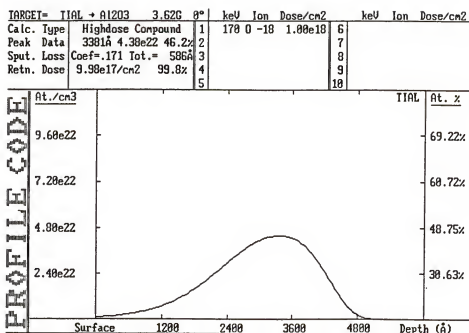


Figure 5-2. The oxygen distribution obtained using the PROFILE code for implantation of $1 \times 10^{18} \text{ } ^{18}\text{O}$ ions/cm² at 170 keV into a TiAl target. In this case it is assumed that all of the implanted oxygen forms alumina. The maximum oxygen concentration predicted is 46.2%.

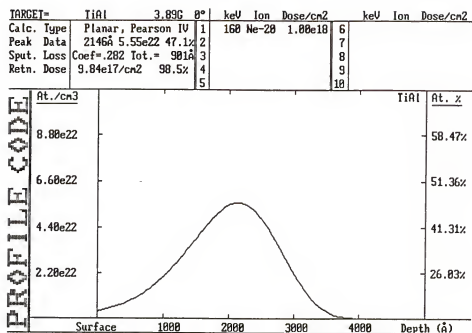


Figure 5-3. The oxygen distribution obtained using the PROFILE code for implantation of 1×10^{18} ^{20}Ne ions/cm² at 160 keV into a TiAl target. The maximum neon concentration predicted is 47.1%.

that of the higher energy peak. An overall decrease in intensity is therefore expected for all of the metal peaks measured in the implanted layer, due to a combination of lower density of metal atoms and peak broadening due to the presence of a high concentration of oxygen. Oxidation of the elements in the matrix is expected to result in a shift in the Al LVV peak to lower energy and a change in the relative magnitude and width of the Ti MVV peaks.

In figures 5-4 A,B and C are shown Auger spectra from a specimen of TiAl implanted with $1 \times 10^{18} \text{ }^{18}\text{O}$ ions/cm² at 164 keV. These figures show a montage of spectra obtained by sputtering the area of interest with Ar for 12 seconds, collecting spectra from each element, and then sputtering further. The total sputter time in this case was eight minutes. By presenting the data in this format the changes that occur in the spectra due to the presence of the implanted oxygen layer can be easily demonstrated. Figure 5-4 A shows the Al LVV peaks. It is immediately obvious that at a level below the surface which corresponds to the implanted oxygen layer, the peak shifts to lower energy and decreases drastically in magnitude. Obviously much of the Al present in the implanted layer has formed an oxide.

The oxidation state of the Ti in the implanted layer is not as clear as that of the Al. Figures 5-4 B and C show the Ti MVV peaks in normal and differential mode respectively. In figure 5-4 B the spectra are skewed to show the relative magnitudes of the normal

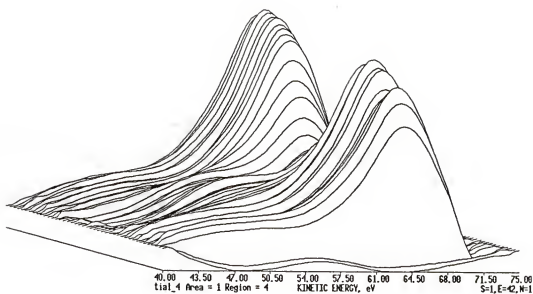


Figure 5-4 A. Montage of Al LVV Auger peaks collected from a depth profile of a specimen of oxygen implanted TiAl. The peaks occurring at the depth of the implanted oxygen decrease in magnitude and shift to lower energy indicating that most of the Al in this region is bound as oxide.

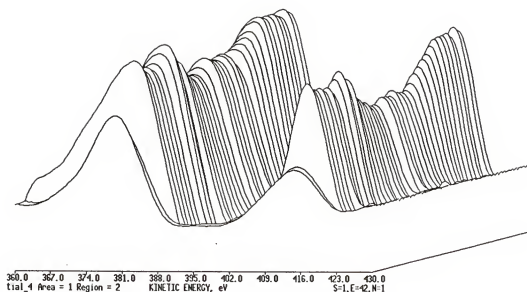


Figure 5-4 B. Montage of Ti LVV Auger peaks collected from a depth profile of a specimen of oxygen implanted TiAl (normal mode). Some variation in intensity is apparent in the Ti spectra from the surface through the implanted region, but no clear energy shift is observed. This set of data indicate that only a limited amount of the Ti present in the implanted layer is bound as oxide.

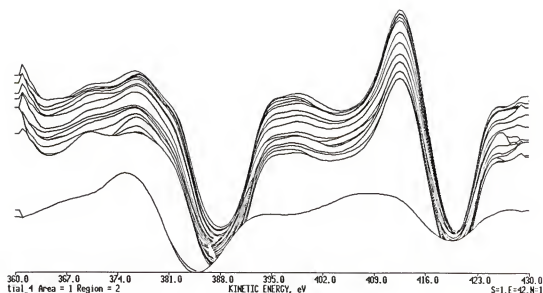


Figure 5-4 C. Montage of Ti LVV Auger peaks collected from a depth profile of a specimen of oxygen implanted TiAl (differential mode). The first spectra at the surface correspond to titanium oxide in the native oxide film. Characteristic of the Auger spectra from Ti oxide is a shift in energy and the intensity of the higher energy peak (on the left) appearing higher than that of the lower energy peak. No such effects are observed in the implanted layer. This set of data indicate that only a limited amount of the Ti present in the implanted layer is bound as oxide.

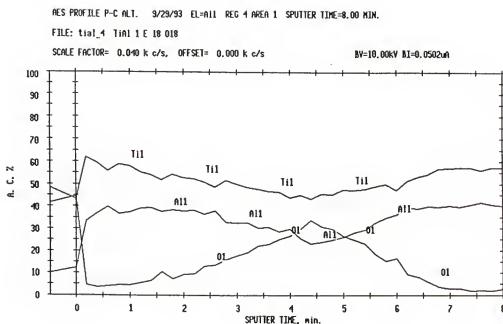


Figure 5-5. Composite depth profile of Auger peak heights collected from a depth profile of a specimen of oxygen implanted TiAl. The implanted oxygen distribution is clearly visible. At the center of the implanted layer the oxygen signal intensity is near that at the surface where a native oxide film is present.

peaks. Although the peak heights vary with depth, the relative magnitudes of the two principal peaks appear to vary simultaneously, whereas if the majority of the Ti were oxidized (as TiO or TiO_2) the lower energy peak should increase at the expense of the higher energy peak. Comparison of the peaks from the implanted region (approximately the center of the figure) with those in the matrix (the back edge of the figure) shows that over much of the depth profile from the surface through the implanted region the lower energy peak shows the greatest intensity. Referring to figure 5-4 C provides additional information. This is the same data as shown in 5-4 B presented in differential mode. The first spectrum shown in this montage is due to the surface oxide. This was determined using XPS to be predominantly TiO_2 . Note the distinct shift both in peak positions and energy compared to the other spectra. If the lower energy peaks are compared individually a shift of 1 eV is evident (from 386 to 385 eV) however; as can be seen in the figure 5-4 C, at no position does a drastic shift in peak positions or magnitude occur. The slight changes in peak shape and energy that are evident are taken to mean that the primary signal collected in all cases is still due to Ti metal but in the implanted region a fraction of the Ti atoms present are bound to oxygen. A composite Auger depth profile produced from the same data as figs. 5-4 is shown in figure 5-5. The expected overall decrease in metal signal intensity is evidenced under the oxygen distribution. Note that the Al signal at the surface is much lower than that of the Ti, which confirms the surface layer, as consisting primarily of titanium oxide.

To summarize: the Auger data from as-implanted TiAl indicate that in the as-implanted state much of the Al in the center of the implanted region is bound to oxygen

but most of the Ti present is still metallic. Recalling that the oxygen concentration achieved by implantation was predicted by PROFILE to be approximately 50% (maximum). If the Ti:Al ratio remains 1:1 and if all of the Al at under the maximum in the implanted distribution is bound as Al_2O_3 , then in this region the remaining O to Ti ratio would be 1:2. The Ti may therefore be present primarily as oxygen saturated metal.

Secondary Ion Mass Spectrometry

Introduction

The same SIMS parameters were used for the TiAl specimens as were used for the NbAl₃. The principal secondary ions of interest in this case were $^{16}\text{O}_2^+$, $^{18}\text{O}_2^+$, $^{27}\text{Al}^+$, Ti^+ , and Ti_2^+ . The dimer ions were collected because the monomer signal tended in some cases to saturate the detection system. In addition AlO^+ and TiO^+ profiles were collected in order to provide corollary information. The same general comments on interpretation of SIMS spectra made in the NbAl₃ section apply here as well. The TiAl specimens were fine-grained and did not show any porosity in the areas examined, consequently the background levels of ambient oxygen species were lower than those observed with NbAl₃.

As-Implanted TiAl

A SIMS depth profile from a specimen of TiAl as-implanted with 10^{18} ^{18}O ions/cm² is shown in figure 5-6. Two different Ti species are shown as well as the Al, ^{18}O and ^{16}O profiles. Under the implanted peak a maximum in the Ti signal occurs while minima flanked by local maxima are observed in both the Al^+ and Ti_2^+ profiles. The oxygen distribution is relatively flat across at the maximum, indicating that an oxygen saturated

region has been formed. This saturated region correlates to the maximum in the Ti^{1+} signal and the minima in the Al^{1+} and Ti^{2+} signals. The small local maxima in the Ti^{2+} and the Al^{1+} correspond to the same net oxygen signal intensity level. Under the implanted peak the two oxygen species mirror each other, resulting in a nearly constant oxygen concentration. The source of this ^{16}O distribution is interesting in itself. In the Auger spectra discussed above, only the implanted oxygen peak was detected. Since Auger analysis is not sensitive to particular isotopes, if this distribution was present when the specimen was examined in the Auger spectrometer, the spectra would have indicated a constant concentration of oxygen down to a depth beyond the tail of the implanted distribution. This might lead to the conclusion that there is a difference in the oxygen distribution between the specimens examined in Auger and SIMS but the Auger and as-implanted SIMS spectra presented in figures 5-4 through 5-6 were measured from the same specimen. The ^{16}O detected distribution shown in figure 5-6 must therefore be due to an instrumental effect of the SIMS. This occurs due to the high background concentration of oxygen in the SIMS. While the absolute vacuum in the Auger system is at 5×10^{-9} to as high as 10^{-10} torr with an extremely low oxygen background due to the use of Ti gettering pumps, the vacuum in the SIMS during profiling is on the order of only 10^{-7} torr, with a fairly high oxygen level due to the contamination of the system with oxygen sputtered from samples, as well as from the use of ^{16}O as a primary ion species. The background oxygen level in the SIMS was therefore sufficiently high to react with the clean TiAl surface as it was being sputtered. Note that the ^{16}O profile decays rather slowly and appears to approach a background level two orders of magnitude higher than ^{18}O . This effect is not as noticeable in the oxidized

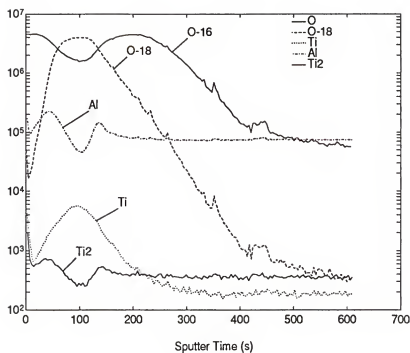


Figure 5-6. SIMS depth profile Ti, Al and O species measured from a specimen of TiAl as-implanted with 1×10^{18} ^{18}O ions/cm². The ^{16}O distribution appears to be primarily due to the high oxygen background in the spectrometer which results in sufficient oxygen present to react with the specimen while the surface is being sputtered. Note that this distribution reaches a minimum under the implanted oxygen peak.

and annealed specimens due to the use of Al^{16}O^+ and $^{16}\text{O}_2^+$ as the detected secondary ion species rather than $^{16}\text{O}^+$ as detected in the as-implanted specimen. In any case the relation between the net concentration of oxygen detected in this specimen and the position of the extrema in the metal profiles is significant. It indicates that these extrema mark the interfaces of a defined oxide layer. Under the implanted peak the metal is practically saturated with oxygen by the implanted species (based on the ^{16}O intensity decreasing by approximately a factor of three in this region.). This result also suggests that dissolved oxygen will rapidly react with the unoxidized metal both within and immediately outside of the implanted region to form a continuous oxide layer. These results taken together with the Auger data prove that the objective of forming a continuous oxidized layer by implantation of oxygen has been met with the TiAl.

Annealed Oxygen-Implanted TiAl

All of the oxidation and annealing experiments were conducted at 1000°C . Annealing experiments utilized an atmosphere of UHP argon passed through a gettering furnace then over the specimen which was suspended from a sapphire rod in a vertical tube furnace. Oxidation experiments were performed in an atmosphere of Ar-0.1% O_2 using the same furnace arrangement. SIMS analysis was conducted only with specimens exposed for short durations as the growth of uneven scales on the surface of the specimens at longer times ruins the depth resolution of the SIMS measurements.

Figures 5-7 and 5-8 show depth profiles measured from non-implanted and implanted regions of a specimen of TiAl annealed for 15 minutes. As in the case of the

NbAl₃ some limited oxidation appears to have occurred during the annealing of this specimen. Considering that the ¹⁶O background in the SIMS is rather high, there nonetheless appears to be significantly less oxygen penetration into the implanted surface compared to the non-implanted region. The fine details in the metal profiles under the implanted peak appear to have been lost due to the annealing. There are still small local maxima and minima in the Ti₂¹⁺ profile but they are less distinct due to the broadening of the SIMS profiles apparently caused by diffusion of both the implanted oxygen and the metal species. There is a surface maximum in the Ti simultaneous with a drop in the Al signal intensity which indicates the formation of titanium oxide at the surface of this specimen. The Al signal increases below the surface while the Ti signal declines suggesting that aluminum diffusion toward the surface is enhanced in the implanted specimen. Neither of these features is particularly evident in the non-implanted profile. Comparison with the as-implanted profile of figure 5-6 indicates that the near surface features in both the Ti and Al profiles are due to local diffusion of these species out of the implanted region toward the surface. The persistence of the implanted peak in maintaining a signal intensity level above that of the ambient oxygen indicates that over the short term the implanted layer is stable with respect to oxygen diffusion. The extended tail of the ¹⁸O distribution into the substrate indicates that some diffusion of the implanted species is occurring, however this effect is due at least partially to oxygen which is sputtered from the specimen and recombines with the fresh surface, as observed in figure 5-6 as well.

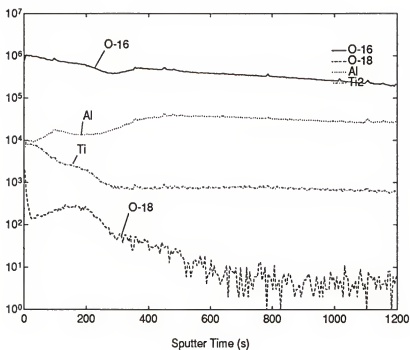


Figure 5-7. SIMS depth profile from the non-implanted region of a specimen of TiAl annealed for 8 minutes in H-P Ar at 1000° C.

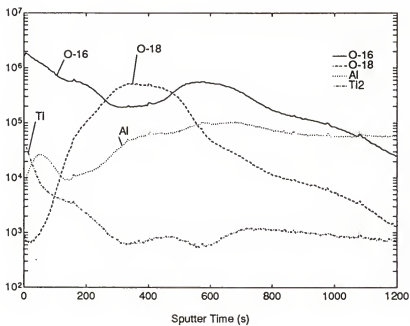


Figure 5-8. SIMS depth profile from the ^{18}O implanted region of the same specimen profiled in 5-7 above. Recalling that much of the ^{16}O distribution is due to background, the penetration of ambient oxygen is lower in this specimen and the distribution of Ti and Al species is changed

Oxidized Oxygen-Implanted TiAl

For SIMS analysis oxidation experiments had to be as brief as possible in order to avoid the formation of thick surface oxides. The resulting rough surface causes the SIMS profiles to broaden significantly, with a resulting loss of information. In order to determine the optimum exposure duration for oxidation experiments, non-implanted specimens were exposed for time periods ranging from 90 seconds to 30 minutes. The shortest exposures resulted in non-uniform scales, possibly due to the effects of uneven heating. At times greater than 5 minutes the scales appeared to be a uniform light gray to white. As the exposure duration increased the scales grew thicker and the roughness of the surface increased. It was determined that an exposure of eight minutes was optimum to allow enough time for the specimen to completely reach 1000° C and be exposed for at least 5 minutes at this temperature. In addition a Ne implanted specimen was exposed under exactly the same conditions, in order to determine whether any of the observed effects were due to radiation damage rather than the presence of the implanted oxide layer.

Three different regions were identified for SIMS analysis on the oxygen and neon implanted samples. These features are visible in the macrograph of figure 5-9. The implanted and non-implanted regions are separated by a band referred to herein as the transition region. The transition region at the edge of the implanted area is due to the lack of perfect collimation of the ion beam. This area has been implanted but at a much lower dose than in the main implanted area. This region is of interest because after the oxidation exposure it appeared to have produced the thinnest scale of the three regions, based on visual inspection, while the implanted region appeared to be covered with a



Figure 5-9. Macrograph of specimens of TiAl implanted with ^{20}Ne (left) and ^{18}O (right) at a fluence of 1×10^{18} ions/cm². Subsequently each was oxidized for 8 minutes. The implanted, non-implanted, and transition regions are clearly visible, (the implanted area lies within the semicircle defined by the transition area) as are numerous SIMS craters (the small square spots).

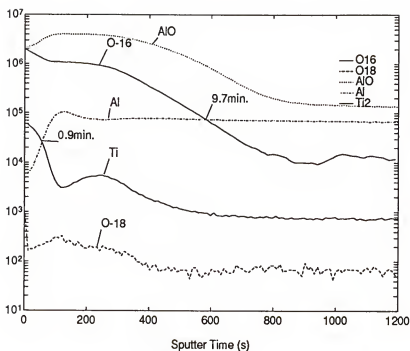


Figure 5-10. SIMS depth profiles from the non-implanted region of a specimen of TiAl oxidized for 8 minutes at 1000°C.

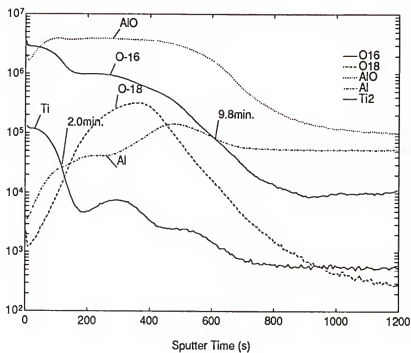


Figure 5-11. SIMS profiles from the ^{18}O implanted region of a specimen of TiAl oxidized for 8 minutes at 1000°C. The broad Ti distribution near the surface is consistent with formation of a rutile surface oxide.

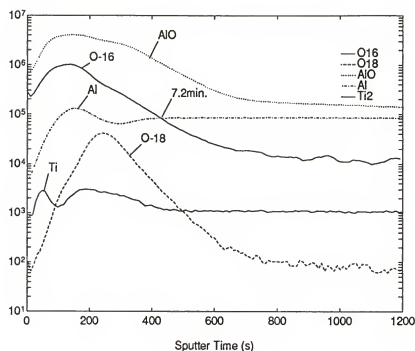


Figure 5-12. SIMS depth profiles from the transition region between the non-implanted and implanted regions of the same specimen of TiAl oxidized at 1000° C for 8 minutes which was used for figures 5-10 and 5-11 above. This region was partially implanted and seems to have formed the thinnest oxide layer, based on the apparent depth of the AlO and ^{16}O distributions.

continuous white oxide layer. SIMS profiles taken from these three regions are shown in figures 5-10, 5-11, and 5-12. Comparing 5-10 with 5-11 it seems readily apparent that the presence of the implanted layer did not reduce the transport of oxygen into the surface of the specimen. A convenient point of reference is the cross over of the ^{16}O and Al profiles. These occur at virtually the same depth in these two figures. The ^{18}O peak is now below the level where it formerly intersected the ^{16}O profile. Both of these features indicate that oxygen transport through the implanted region is largely unaffected by the presence of the implanted oxygen layer. There is a significant difference in the appearance of the Al and Ti profiles between the two figures. In both cases there is a maximum in the Ti intensity at the surface and a corresponding minimum in Al, indicating formation of a titanium oxide species at the surface. In the implanted area however the maximum in the Ti signal is greater and it extends further into the surface. The minimum in the Al profile in the implanted specimen is not only lower near the surface but it also increases much more gradually toward the matrix value. These features indicate that the presence of the implanted layer actually encourages the formation of titanium oxide on the surface of the implanted region. This is of course precisely opposite the desired result. Nonetheless the evidence appears to show that the implanted layer does not improve the oxidation kinetics of TiAl, and may in fact make the situation worse. Examination of figure 5-12 initially leads to a different conclusion. In the transition region apparently the oxide layer is, as it initially appeared, thinner than in either the main implanted area or in the non-implanted area. Not only does the ^{16}O profile extend less into the surface than in either of the other areas, but the positions of the metal profiles are reversed. In the transition region both the

Al and Ti profiles are low at the surface, but the Al profile is at all times at a higher level than the Ti, a phenomenon which is not observed in either of the other areas. The Al peak reaches a local maximum under the ^{16}O peak, which has decreased by about a factor of three by the point where the maximum in the implanted peak is reached. The ^{18}O peak is a factor of ten lower than in the main implanted region, but it appears more symmetrical, indicating possibly that less diffusion of the implanted species occurs at a lower dose of implanted oxygen. This latter possibility does not seem to be particularly likely based on the results of nearly identical experiments conducted using samples implanted at a lower dose 2×10^{17} ^{18}O ions/cm² and oxidized for 5 minutes. For comparison these are shown in figures 5-13 and 5-14. These appear to be qualitatively very similar to 5-11 and 5-12, the major difference being solely in the magnitude of the implanted peak. Once again the Ti profile near the surface is broader in the implanted region and the implanted ^{18}O profile trails off into the bulk. The apparently decreased oxidation rate in the transition region is therefore not explained by a favorable lower implantation dose resulting in increased formation of alumina. Apparently the oxygen implantation results in more rapid growth of titanium oxide scales on the implanted surface. The thinner scale in the transition region may therefore be attributed to the growth of a rutile layer which is more protective than the oxide formed on the non-implanted region but is not as thick as that on the implanted region. Since this layer can be seen to form on the surface side of the implanted oxygen distribution, it apparently grows by Ti cation transport to the scale/gas interface. This mechanism presumably would be accelerated by an increase in defect concentration in the metal lattice below the scale. Additional evidence of the operative oxidation mechanism in

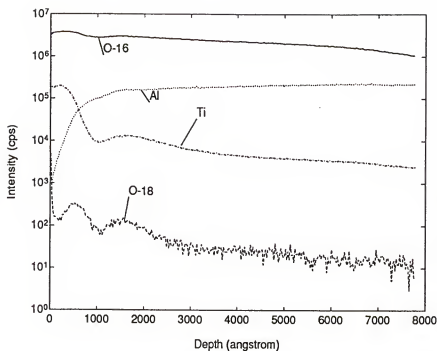


Figure 5-13. SIMS depth profile measured from the non-implanted region of a specimen of TiAl oxidized for 5 minutes at 1000°C . Note the prominent maxima in the Ti distribution near the surface.

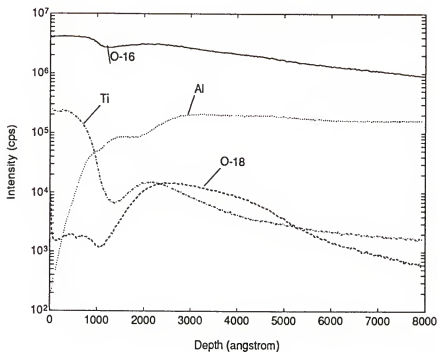


Figure 5-14. SIMS depth profile from the implanted region of the same specimen profiled in fig. 5-13. This specimen was implanted with $2 \times 10^{17} \text{ }^{18}\text{O ions/cm}^2$ at 160 keV. Note that the Ti distribution near the surface is broader than in the non-implanted region.

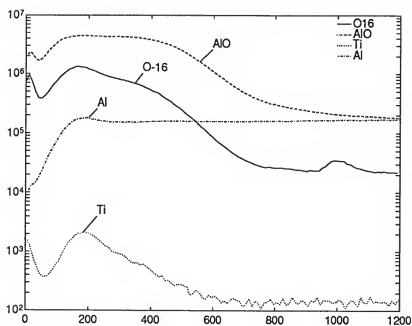


Figure 5-15. SIMS depth profile from a specimen of TiAl oxidized for 8 minutes at 1000° C. This is provided for comparison to fig. 5-16 below.

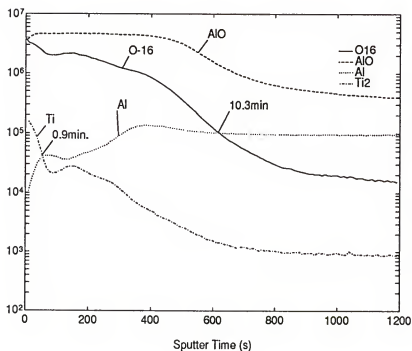


Figure 5-16. SIMS depth profile from the implanted region of a specimen of TiAl implanted with 1×10^{18} ^{20}Ne ions/cm² at 160 keV. This implant was intended to simulate the radiation damage produced by the oxygen implants.

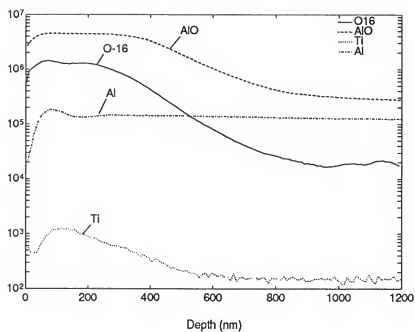


Figure 5-17. SIMS profile of from the transition region of a specimen of TiAl implanted with $1 \times 10^{18} \text{ }^{20}\text{Ne}$ ions/cm² and subsequently oxidized for 8 minutes at 1000° C.

the implanted specimens is provided by the results of the Ne implants. If increased cation transport is the explanation for the effects seen on the oxygen implanted surfaces, then inert ion implants should produce sufficient lattice damage to see similar effects. Figures 5-15, 5-16, and 5-17 show the non-implanted, Ne implanted, and transition region profiles taken from the Ne implanted specimen oxidized for 8 minutes at 1000° C. The Ne profile could not be collected effectively using negative SIMS however the metal profiles and oxygen profiles are presented for comparison to figures 5-12 through 5-14. It is important to realize that in this specimen there was more surface topography introduced into the implanted region by the neon implant than was observed in the oxygen implant. The differences observed between the profiles of the three regions do however follow the same pattern as those taken from the oxygen implanted specimen. The implanted region exhibits the highest and broadest near surface Ti peak. The non-implanted region does not show this feature as distinctly however the Ti and Al profiles do respectively increase and decrease near the surface. In the transition region the Ti and Al both appear to decrease near the surface. The pattern of these effects indicates that the increased oxidation observed in the implanted region of the oxygen implanted specimen is due to increased Ti transport to the surface through the near surface region which has been disordered to some extent by the implantation process. This also explains the results reported by Meier et al.¹³ where they observed that implantation of Al, Si, N, and C resulted in accelerated oxidation rates in γ TiAl based alloys resulted in accelerated oxidation rates.

The conclusion drawn from the results of these experiments is that oxygen implantation will not result in an improvement in the oxidation resistance of TiAl. To the

contrary, the radiation damage introduced by the implantation process may serve to accelerate the formation of Ti based oxides which are non-protective at the temperatures where TiAl might be used to best advantage. Therefore no longer term experiments were conducted on high-dose oxygen implanted TiAl.

CHAPTER 6

OXYGEN IMPLANTED NiAl

Ion Implantation

The same discussion of implant parameters covered in chapter 4 is relevant here. Once again the implantation dose used was 1×10^{18} ^{18}O ions/cm², in this case at an accelerating energy of 100 keV. In NiAl this resulted in a calculated peak oxygen concentration of 47%. The calculated profile is shown in figure 6-1. Assuming all of the oxygen was bound to Al, a concentration of 30 at. % should be sufficient to form a layer in which all of the aluminum is oxidized. The additional 17% oxygen is then available to bind to Ni atoms thus resulting in a layer consisting of aluminum oxide, nickel oxide, and metallic nickel. The much lower free energy of formation of Al_2O_3 compared to NiO makes this result much more likely than the case of TiAl where the metal species could be expected to compete for the implanted oxygen.

Since Ne implants had resulted in excessive surface damage on NbAl₃ and TiAl substrates, no Ne implants were performed with NiAl. Carbon implants were performed as part of a parallel investigation into diffusion measurements using implanted tracers (the details of which are outside the scope of this work). The carbon implants were made at the same accelerating energy but at a fluence of 2×10^{17} . Under the conditions discussed herein the C implanted surfaces are treated as simulations of the implantation radiation damage.

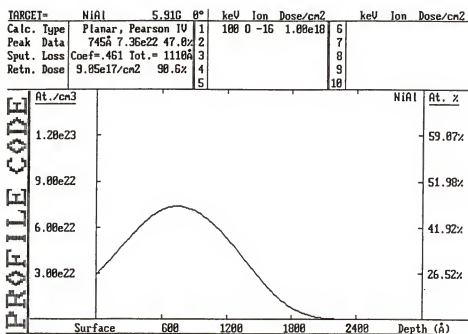


Figure 6-1. Implanted oxygen distribution calculated using PROFILE for ^{16}O implanted into a NiAl target at a fluence of 1×10^{18} ions/cm 2 and an accelerating energy of 100 keV.

NiAl was the only material studied in this project which was available in single crystal form. The use of single crystal specimens simplifies the interpretation of depth profiles as no potential complications are introduced by oxygen transport down grain boundaries, variable oxidation rates due to the orientation of particular grains, or sputter rates varying due to grain orientation. In order to further minimize variability between samples, all of the SIMS specimens for oxidation and annealing experiments discussed in this report were taken from the same piece of material.

A 40mm diameter disk cut from a single crystal at the [110] orientation was polished to a 1 μ finish on both sides prior to implantation. One side was implanted with 1×10^{18} ^{18}O ions/cm² at 100 keV. The other side was implanted with 1×10^{17} ^{12}C ions/cm² at 100 keV. Subsequently the disc was sectioned into eight pie-shaped wedges for use in the experiments. This technique allowed practically identical specimens to be examined in the as-implanted state and after various annealing and oxidation treatments. Each specimen therefore provided data for three different conditions: non-implanted, O-implanted, and C-implanted.

Due to the availability of identical specimens, a larger number of annealing experiments were conducted with NiAl than with TiAl or NbAl₃. Specimens were annealed for 5 minutes, 15 minutes, and 1 hour, all at 1000° C in Ar-10% H₂. Oxidation experiments were conducted for 1, 16, and 42 hours. SIMS analysis of the 42 hour oxidation experiment was possible due to the very thin oxide scale grown on NiAl during isothermal oxidation. A cyclic oxidation experiment in Ar-20% O₂ was conducted with a specimen implanted with 1×10^{18} ^{16}O ions/cm² on one side. This experiment was the only

one to produce precision TGA data, due to the use of the Cahn TG-171 microbalance in the Materials Corrosion and Environmental Effects Laboratory in the MST-6 division at Los Alamos National Laboratory.

Auger Electron Spectroscopy

Auger spectroscopy was used to characterize the oxidation state of the elements in the implanted layer. As previously discussed, the Al Auger peaks exhibit distinct shifts to lower energies when going from the metallic to the oxide state. Unfortunately Ni when oxidized exhibits no significant energy shift and only subtle differences in peak shape and magnitude. The changes in peak shape that might occur with Ni are masked by changes in atomic density and minor instrumental effects during depth profiling. Consequently the changes observed in the Ni Auger spectra are those due to significant variations in atomic concentration with depth. Therefore it is only possible to determine the oxidation state of Al in the implanted specimens.

Auger depth profiling was performed on NiAl specimens both in the as-implanted state and after a 5 minute anneal in Ar-4.62% H₂ at 1000° C. In the as-implanted state the Al LVV peaks exhibited a small shift in the implanted state, with a significant decrease in intensity due primarily to the lower atomic density of aluminum in the implanted layer. This suggests that in the as-implanted state that the Al was only partially oxidized or that some intermediate oxide state was formed sharing the oxygen between Al and Ni, with possibly some unoxidized material present as well. Figure 6-2 shows a composite depth profile measured from an as-implanted specimen of NiAl. The vertical axis on this plot has been converted to atomic concentration. The profile labeled Al₂ is the intensity of the Al

LVV peak shifted 2 eV, while the profile labeled AL3 is the intensity of the metallic Al LVV peak centered at 64 eV. The profile labeled Ni1 is the variation in intensity of the Ni LMM peak with depth. Note that the intensity of the Ni peak decreases significantly under the implanted oxygen distribution due once again to a decrease in atomic density.

The Auger spectra from the specimen annealed for 5 minutes at 1000° C appeared very different from the as-implanted results. A composite depth profile from the annealed specimen is shown in figure 6-3. Four distinct regions may be observed. The surface consists of nearly continuous aluminum oxide. The second layer just below the surface is unoxidized NiAl. (This layer is not visible in the SIMS profiles discussed below due to the slow decrease in oxygen background in the SIMS after sputtering an oxide layer.) The third layer corresponds to the implanted region. Based on the energy shifts observed in the Al LVV peak this layer consists of aluminum oxide with dissolved Ni. The fourth layer is the unoxidized NiAl substrate. The Ni distribution in the implanted layer suggests that Ni is being rejected from the implanted layer into the unoxidized NiAl layers on either side. This would account for the Ni minima on either side and is consistent with low solubility of Ni in Al_2O_3 . A montage of the Al LVV spectra from this same specimen is shown in figure 6-4. The first surface spectrum has been removed for clarity. Peaks for both the Al oxide and metal states appear just below the surface. The oxide peak disappears as the fraction of aluminum in the metal state increases. Deeper into the specimen the metal peak decreases drastically as apparently all of the aluminum in the implanted layer is oxidized. Taken together these data show conclusively that after a very brief anneal the implanted layer consists primarily of aluminum oxide with Ni present in solution or as a compound.

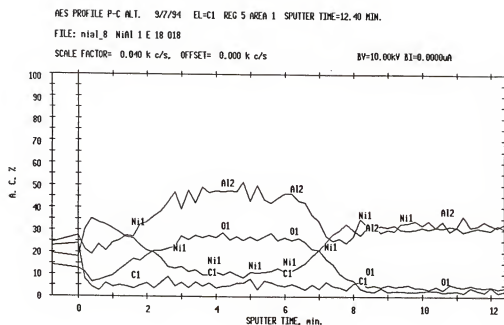


Figure 6-2. Composite Auger depth profile from an as-implanted specimen of NiAl. The profile labeled Al2 is the intensity of the shifted Al LVV peak while that labeled Al3 is the Al LVV metal peak intensity.

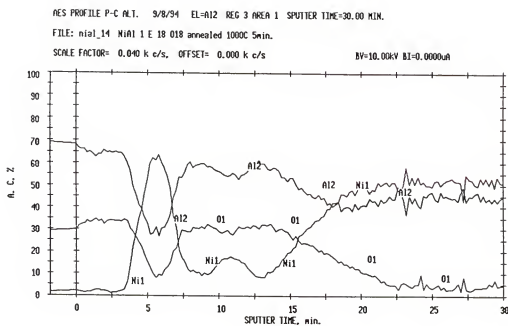


Figure 6-3. Composite Auger depth profile from an oxygen implanted specimen of NiAl which was annealed for 5 minutes at 1000° C 5 in Ar-4.62%H₂. A layered structure has evolved which is consistent with the formation of a continuous oxide layer from the implanted region.

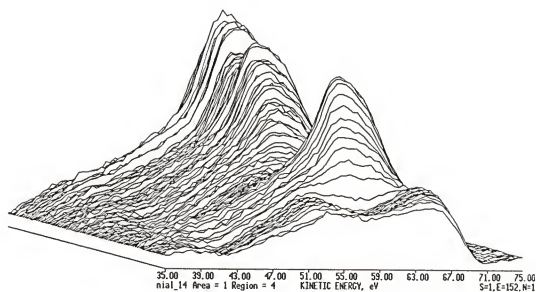


Figure 6-4. Montage of Auger spectra of the Al LVV Auger peak, measured from the specimen of oxygen-implanted NiAl annealed for 5 minutes at 1000° C.

X-Ray Diffraction

Since the substrate utilized in all of these experiments was (110) oriented single crystal NiAl, it is not surprising that the only peak observed in the as-implanted material was the [110] NiAl peak at $44.369^\circ 2\theta$.⁷⁸ This peak is shown in figure 6-5. In the implanted and annealed specimen a second distinct peak appeared at approximately (44.2°) which seemed to shift slightly depending on the duration of the exposure. This pair of peaks, measured from the specimen oxidized for 1 hour, is shown in the XRD pattern of figure 6-6. This was the only additional peak to appear which indicates that the implanted layer crystallized with an epitaxial relationship to the substrate. This peak does not correspond to any binary alumina phase. The best match found for this peak is the [400] peak of NiAl_2O_4 at $44.996^\circ 2\theta$.⁷⁹ The d-spacing of the NiAl [110] planes is 4.083 \AA while that of the NiAl_2O_4 is 8.048 . The lattice spacing of two NiAl cells is within 2.2% of the NiAl_2O_4 if the oxide is growing with its [100] planes parallel to the NiAl [110]. The peak shift may be explained by a combination of the effects of deviation from stoichiometry of the NiAl_2O_4 and mismatch strain at the NiAl/ NiAl_2O_4 interface. Therefore NiAl_2O_4 seems to be the most likely candidate for the oxide grown from the implanted layer. No such effect was observed on the C implanted side, which still showed only the NiAl peak. This same pattern was observed in the specimens oxidized for 42 hours, with 1 additional peak which appears to correspond to the α alumina [113] peak at $43.362^\circ 2\theta$.⁸⁰ The implanted region did not show any characteristic topography, except in small areas which had spalled after 42 hours exposure. The non-implanted areas however did show the whisker topography characteristic of θ alumina. This is shown in figure 6-7.

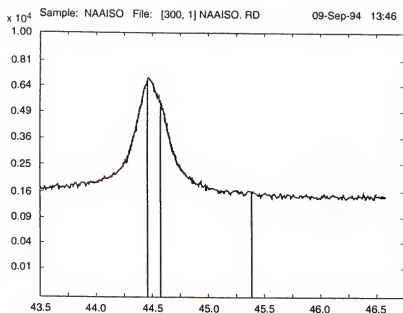


Figure 6-4. XRD pattern from a specimen of (110) NiAl as-implanted with 1×10^{18} ^{18}O ions/cm². The peak corresponds to [110] NiAl and is also the only peak observed in non-implanted specimens or those implanted with C.

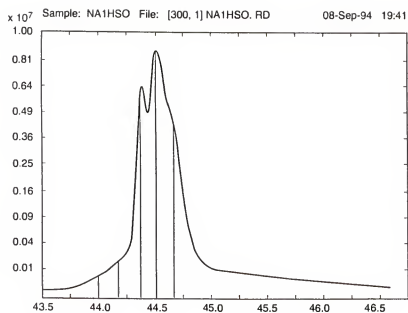


Figure 6-5. XRD pattern from a specimen of (110) NiAl implanted with 1×10^{18} ^{18}O ions/ cm^2 and annealed for 5 minutes at 1000°C . The second peak is due to the recrystallized implanted layer which apparently has a close epitaxial relation to the substrate. No other peaks were observed.

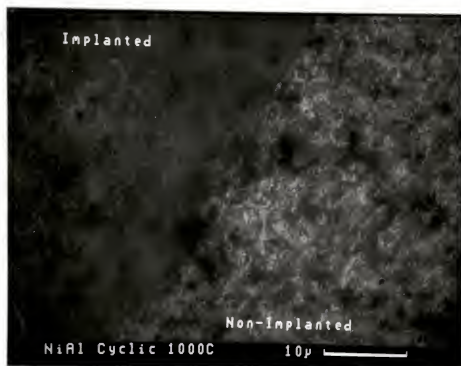


Figure 6-7. SEM micrograph of non-implanted (right) and implanted (left) areas of an oxygen implanted NiAl specimen cyclically oxidized for a total of 16 hours at 1000° C. The non-implanted areas display the whisker morphology characteristic of theta alumina.

Secondary Ion Mass Spectrometry

Introduction

SIMS analysis was performed in all cases using a Cs⁺ primary ion beam. Negative ions were collected for all species. The principal secondary ions of interest were $^{16}\text{O}_2^-$, $^{18}\text{O}_2^-$, $^{27}\text{Al}^-$, and $^{54}\text{Ni}^-$. The dimer ions were collected to reduce interferences and because the monomer signal tended in some cases to saturate the detection system. In addition AlO^- and NiO^- profiles were collected in order to provide corollary information. The superposition of all of these profiles on a single plot is illegible, so in all of the data presented below, the profiles are limited to those species which show the important results most clearly. In some cases multiple plots of data from the same sputter profile are used for clarity. Raw SIMS data is collected as intensity of counts at a given mass as a function of time. At a single primary ion intensity, the detected intensity for a particular element varies as the concentration of the element in the substrate, and the chemical bonding of the element or the matrix of which it is a component. The intensities of different elements vary depending on their ionization and elastic scattering cross-sections which vary with primary ion energy. In most cases negative SIMS depth profiles were collected. Negative profiles maximize the sensitivity for oxygen isotopes, although some metal ion sensitivity is lost. Since the metal ions in this case are from the matrix elements, sensitivity was acceptable. Singly charged ions were collected in all cases except for the oxygen isotopes, for which the singly charged intensity was too high. In the case of C profiles the $^{12}\text{C}_4^{1-}$ species was collected in some cases. The C implanted profiles are presented for comparison to the O implanted and non-implanted profiles. In cases where no important

difference exists, the C implanted profile alone is presented. As was discussed in earlier sections, there is some additional uncertainty in converting the time axis to units of depth because of the potential for sputter rate to change with depth in the specimen. In the case of TiAl and NbAl₃, although this uncertainty exists, no special effort was made to compensate as the uncorrected data showed the important effects. In this case however, the accuracy of the depth scale was improved by sputtering pits for fractions of the time to obtain the complete profile. The depth these pits was subsequently measured in order to determine what, if any, variation in sputter rate there was within the depth of interest on a given sample. This extra effort was considered worthwhile only for the NiAl specimens, given that all other uncertainties in comparison between specimens had been eliminated by the use of a sectioned single crystal for all of the experiments.

As-Implanted NiAl

Figures 6-8 and 6-9 show SIMS profiles collected from the NiAl single crystal as implanted with 1×10^{18} ^{18}O ions/cm². Figure 6-10 shows a profile measured from the opposite side of this same specimen, as-implanted with 1×10^{17} ^{12}C ions/cm². The most significant feature in these three figures is the strong enhancement in Al and to a lesser extent Ni intensity under the implanted oxygen peak. This effect is much less obvious in the C implanted specimen. Note also that in these specimens the ^{16}O signal decreases sharply from the surface to background levels which are much lower than observed in the TiAl or NbAl₃. This is partially due to the lack of grain boundaries and voids containing trapped oxygen in this specimen. This effect also indicates that the oxygen affinity of NiAl

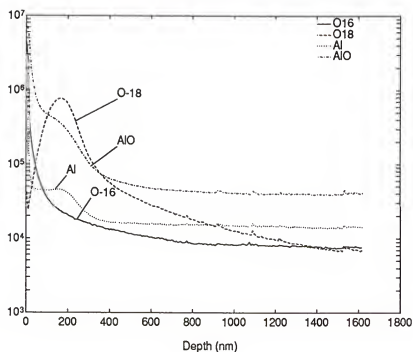


Figure 6-8. SIMS profile showing O and Al species from a specimen of [110] single-crystal NiAl as-implanted with $1 \times 10^{18} \text{ }^{18}\text{O}$ ions/cm² at 100 keV.

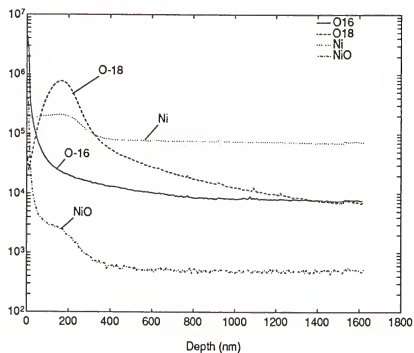


Figure 6-9. SIMS profile showing O and Ni species from a specimen of [110] single-crystal NiAl as-implanted with $1 \times 10^{18} \text{ }^{18}\text{O}$ ions/cm² at 100 keV.

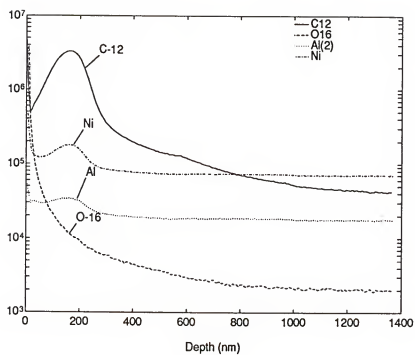


Figure 6-10. SIMS profile showing O, C, Al, and Ni species from a specimen of [110] single-crystal NiAl as-implanted with 2×10^{17} ^{12}C ions/cm² at 100 keV.

is much lower than that of TiAl. Consequently interpretation of the SIMS spectra obtained from the NiAl specimens is much more straightforward than for TiAl. Note also that the implanted profiles are very symmetrical, indicating that no channeling effects occurred during implantation into the single-crystal target..

Annealed Oxygen-Implanted NiAl

All annealing experiments were conducted in Ar-10% H₂ at 1000° C. The surfaces of the specimens were slightly tinted after annealing but remained microscopically smooth. As in the other materials however, the annealing experiments did result in a very low level of oxygen exposure, as revealed by the SIMS profiles. Figures 6-11 through 6-16 are SIMS profiles collected from the specimen of NiAl annealed for 5 minutes. 6-11, 6-12, and 6-15 are profiles of the oxygen and Al species from the oxygen implanted, non-implanted, and carbon implanted areas respectively. 6-13, 6-14, and 6-16 are profiles from the same three areas showing Ni rather than Al species. Examining figure 6-11 it is immediately obvious that a change has occurred in the implanted oxygen profile. The ¹⁸O profile is now flat across most of its peak, with distinctive maxima at either side indicating the presence of interfaces. The maxima are not symmetrical, the one nearer the surface being somewhat sharper, presumably due to slightly better resolution of the interface closer to the surface. This profile indicates clearly that the implanted zone has reordered into a distinct layer buried in the surface of the specimen. Both the Al and Ni species show maxima at the edges of the implanted layer, however the Al is still at a very high level under the implanted peak while the Ni decreases to background (matrix) level. This

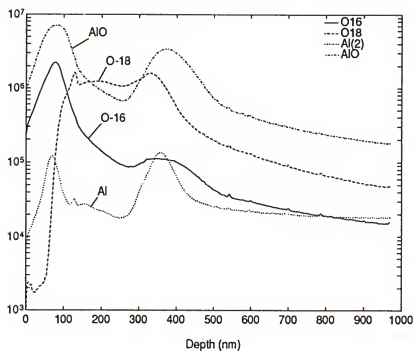


Figure 6-11.
SIMS profile showing O and Al species from a specimen of [110] single-crystal NiAl implanted with 1×10^{18} ^{18}O ions/cm² at 100 keV and subsequently annealed for 5 minutes in Ar-4.62% H₂ at 1000° C.

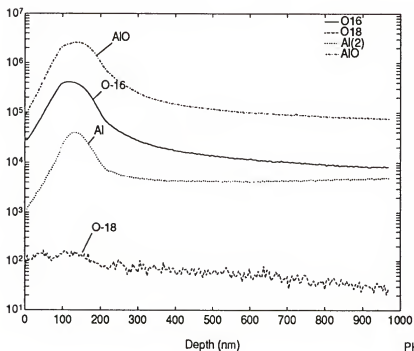


Figure 6-12.
SIMS profile showing O and Al species from a (non-implanted) specimen of [110] single-crystal NiAl annealed for 5 minutes in Ar-4.62% H₂ at 1000° C.

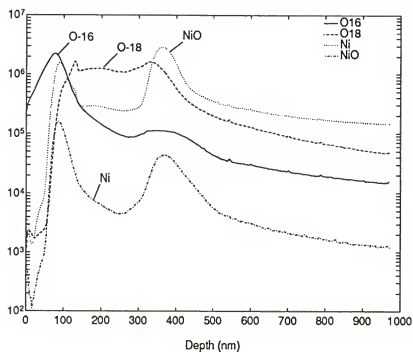


Figure 6-13. SIMS profile showing O and Ni species from a specimen of [110] single-crystal NiAl implanted with 1×10^{18} ^{18}O ions/cm² at 100 keV and subsequently annealed for 5 minutes in Ar-4.62% H₂ at 1000° C.

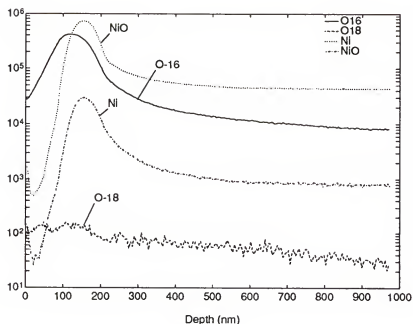


Figure 6-14. SIMS profile showing O and Ni species from a (non-implanted) specimen of [110] single-crystal NiAl annealed for 5 minutes in Ar-4.62% H₂ at 1000° C.

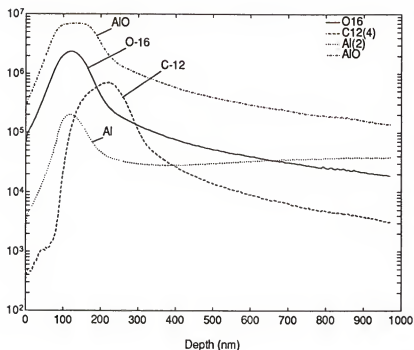


Figure 6-15. SIMS profile showing C, O, and Al species from a specimen of [110] single-crystal NiAl implanted with $2 \times 10^{17} \text{ }^{12}\text{C}$ ions/ cm^2 at 100 keV and subsequently annealed for 5 minutes in Ar-4.62% H_2 at 1000°C .

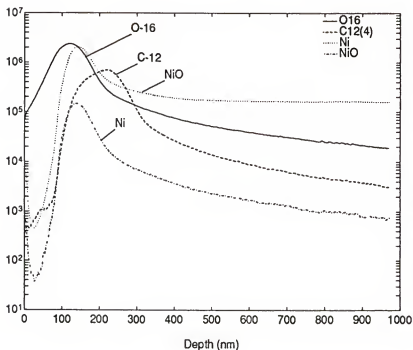


Figure 6-16. SIMS profile showing C, O, and Ni species from a specimen of [110] single-crystal NiAl implanted with $2 \times 10^{17} \text{ }^{12}\text{C}$ ions/ cm^2 at 100 keV and subsequently annealed for 5 minutes in Ar-4.62% H_2 at 1000°C .

indicates that Ni has been rejected from the implanted layer, which contains predominantly aluminum oxide. Toward the surface in all of the profiles the Ni intensity decreases to a minimum while the Al intensity rises to a maximum. This corresponds to the formation of aluminum oxide at the surface. Beyond the implanted profile the ^{18}O intensity decreases slowly indicating that some inward diffusion of the implanted species has occurred. These features are consistent with the Auger depth profiles from the same specimen. In the non-implanted and carbon implanted data, comparison of the oxygen and metal profiles shows that the presence of the carbon implant does not have any noticeable effect. The implanted carbon appears to move with and slightly ahead of the ambient oxygen moving in from the surface, thereby acting as a sort of marker, but no change is observed in the distribution of Ni or Al species. Therefore in the rest of the data presented below only C implanted profiles are shown for comparison.

Figures 6-17 through 6-20 show profiles collected from O and C implanted areas of a specimen of NiAl annealed for 15 minutes. Very little change from the 5 minute anneal has occurred. The surface oxide layer is slightly thicker but in the implanted specimen the ^{16}O peak still tapers off before the maximum in the implanted ^{18}O peak is reached. All of the other features remain essentially the same indicating that the implanted structure shown by the 5 minute profiles is stable and reproducible.

Figures 6-21 through 6-24 show a set of profiles collected from the O and C implanted regions of a specimen of NiAl annealed for 1 hour. The surface in this case sputters more slowly, apparently due to the formation of a layer of alumina sufficiently thick to act as an insulator. The resulting charging causes some spreading and deflection

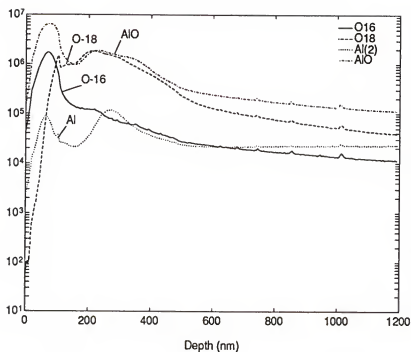


Figure 6-17.
SIMS profile showing O and Al species from a specimen of [110] single-crystal NiAl implanted with 1×10^{18} ^{18}O ions/cm² at 100 keV and subsequently annealed for 15 minutes in Ar-4.62% H₂ at 1000° C.

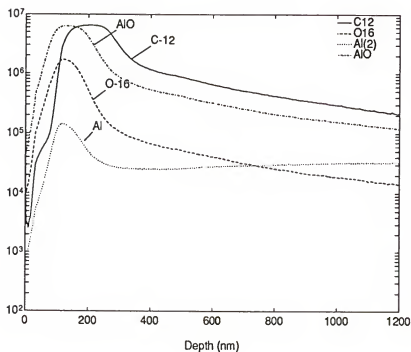


Figure 6-18.
SIMS profile showing O and Al species from a specimen of [110] single-crystal NiAl implanted with 2×10^{17} ^{12}C ions/cm² at 100 keV and subsequently annealed for 15 minutes in Ar-4.62% H₂ at 1000° C.

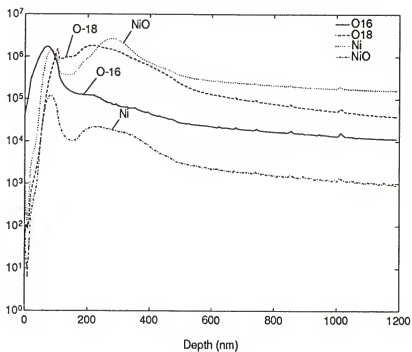


Figure 6-19. SIMS profile showing O and Ni species from a specimen of [110] single-crystal NiAl implanted with 1×10^{18} ^{18}O ions/cm² at 100 keV and subsequently annealed for 15 minutes in Ar-4.62% H₂ at 1000° C.

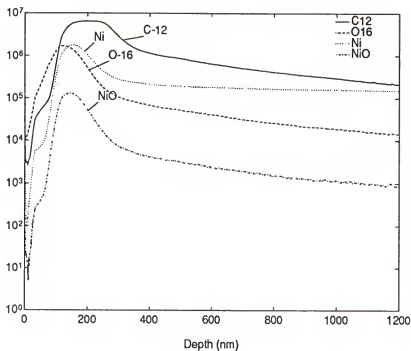


Figure 6-20. SIMS profile showing C, O and Ni species from a (non-implanted) specimen of [110] single-crystal NiAl implanted with 2×10^{17} ^{12}C ions/cm² at 100 keV and subsequently annealed for 15 minutes in Ar-4.62% H₂ at 1000° C.

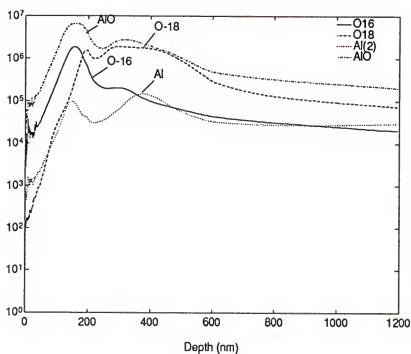


Figure 6-21. SIMS profile showing O and Al species from a specimen of [110] single-crystal NiAl implanted with 1×10^{18} ^{18}O ions/cm² at 100 keV and subsequently annealed for 1 hour in Ar-4.62% H₂ at 1000° C.

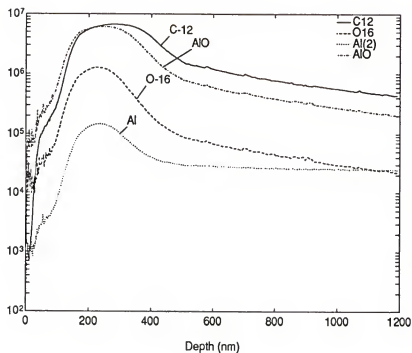


Figure 6-22. SIMS profile showing C, O, and Al species from a specimen of [110] single-crystal NiAl implanted with 2×10^{17} ^{12}C ions/cm² at 100 keV and subsequently annealed for 1 hour in Ar-4.62% H₂ at 1000° C.

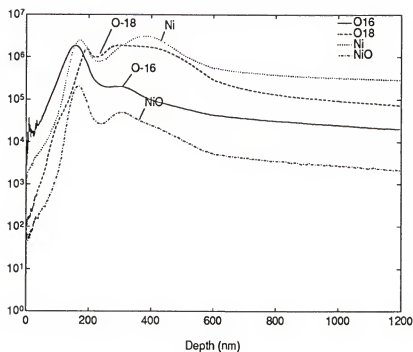


Figure 6-23. SIMS profile showing O and Ni species from a specimen of [110] single-crystal NiAl implanted with 1×10^{18} ^{18}O ions/cm² at 100 keV and subsequently annealed for 1 hour in Ar-4.62% H_2 at 1000° C.

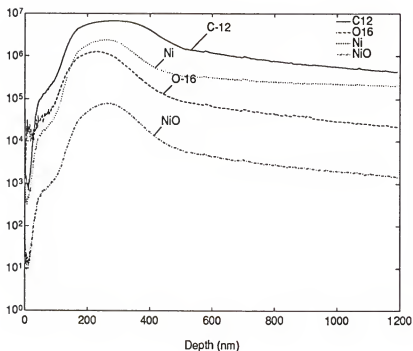


Figure 6-24. SIMS profile showing C, O, and Ni species from a specimen of [110] single-crystal NiAl implanted with 2×10^{17} ^{12}C ions/cm² at 100 keV and subsequently annealed for 1 hour in Ar-4.62% H_2 at 1000° C.

of the primary ion beam. The near surface interface of the implanted oxygen profile is still distinct, but the second peak is no longer clearly visible, due to a combination of oxygen diffusion and decreasing depth resolution due to the changes in sputtering rate. The Ni profile now shows a larger peak near the surface, indicating that some concentration of nickel is occurring due to preferential oxidation of Al at the surface and under the implanted peak. Nonetheless the major features visible after 5 minutes are still apparent in the 1 hour anneal, showing that the implanted layer is stable for up to 1 hour, and therefore may be expected to have a noticeable effect on the initial scale formation under strongly oxidizing conditions.

SIMS of Oxidized Oxygen-Implanted NiAl

Two oxidation experiments were conducted which were subsequently analyzed using SIMS. Both experiments utilized an atmosphere of 0.1% O₂ in UHP Ar. The first experiment was for a duration of 1 hour, the second for 42 hours. Due to the very low weight gains shown by NiAl under isothermal oxidation, less than 1 mg total in 42 h, and the fact that these specimens were only implanted on one side, the TGA data was uninformative. However the same slow scale growth kinetics did allow SIMS analysis of the 42 h exposure. T

Figures 6-25 through 6-28 show SIMS profiles collected from oxygen and carbon implanted regions of a specimen of NiAl oxidized for 1 hour at 1000° C. The x-axis has not been converted to a depth scale because of the uneven surface of the non-implanted regions. Comparison of the profiles of the oxygen implanted areas with the annealed profiles reveals a number of similarities. The pair of maxima in the metal profiles and the

^{18}O profile, identified in the annealed samples as showing the boundaries of the implanted region, are clearly visible present in the profiles from the oxidized specimen. Unlike the annealed specimens however, the ^{16}O profile in the oxygen implanted specimen also shows the same interface maxima. This indicates that the structure of the implanted layer is stable under oxidation, but a significant amount ^{16}O has become part of the structure, either due to oxidation of uncombined metal present in the implanted layer, or which has diffused in from the matrix, or by replacement of ^{18}O . The decrease in intensity of the ^{18}O peak (relative to that observed in the annealed specimen profile of figures 6-21,23) suggests that some diffusion of the implanted species has occurred while atmospheric oxygen has moved into the lattice. The persistence of the interface maxima shows that the structure precipitated by the implanted oxygen is stable, even if a large fraction of the implanted species is replaced or augmented by oxygen diffused in from the ambient. Compared to figures 6-26 and 6-28 (profiles from the C implanted region) the depth penetration of the ^{16}O species is less in the implanted region. This is based on considering the centroid of the inner peak of the AlO or ^{16}O distribution to represent the effective position of the scale/metal interface.

Finally the specimen oxidized for 42h was also profiled using SIMS. Although the profiles are much less distinct due to increased surface topography, there are clear differences between the O and C implanted profiles. Figures 6-29 and 6-30 show profiles of the Al, O and C species from this specimen. The distinct interface structure in the oxide is no longer visible, however the ^{18}O profile is still clearly present. The ^{18}O intensity has decreased by nearly two orders of magnitude but the implanted surface still has produced

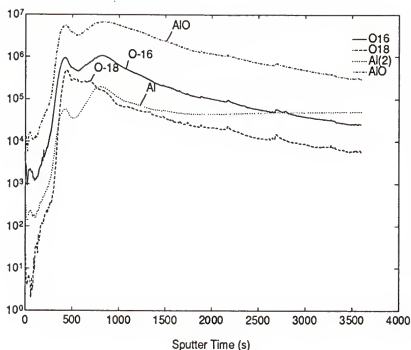


Figure 6-25.
SIMS profile
showing O, and Al
species from a
specimen of [110]
single-crystal NiAl
implanted with
 1×10^{18} ^{18}O
ions/ cm^2 at 100
keV and
subsequently
oxidized for 1
hour at 1000°C .

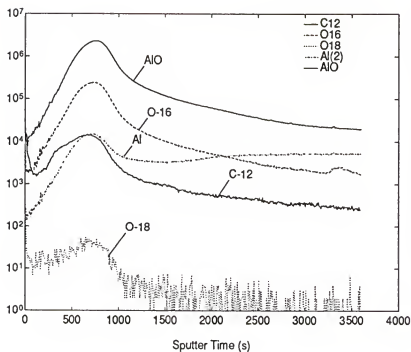


Figure 6-26.
SIMS profile
showing C, O, and
Al species from a
specimen of [110]
single-crystal NiAl
implanted with
 2×10^{17} ^{12}C
ions/ cm^2 at 100
keV and
subsequently
oxidized for 1
hour at 1000°C .

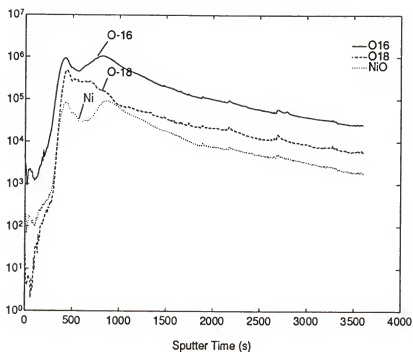


Figure 6-27.
SIMS profile showing O, and Ni species from a specimen of [110] single-crystal NiAl implanted with $1 \times 10^{18} \text{ }^{18}\text{O}$ ions/cm² at 100 keV and subsequently oxidized for 1 hour at 1000° C.

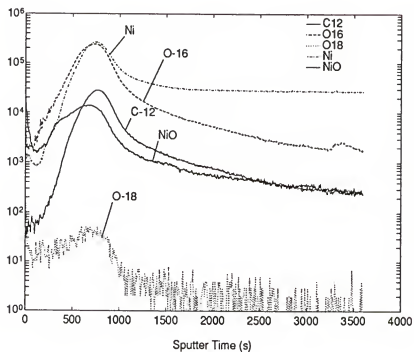


Figure 6-28.
SIMS profile showing C, O, and Ni species from a specimen of [110] single-crystal NiAl implanted with $2 \times 10^{17} \text{ }^{12}\text{C}$ ions/cm² at 100 keV and subsequently oxidized for 1 hour at 1000° C.

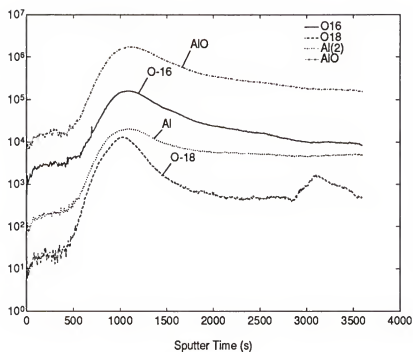


Figure 6-29.
SIMS profile showing O, and Al species from a specimen of [110] single-crystal NiAl implanted with 1×10^{18} ^{18}O ions/cm² at 100 keV and subsequently oxidized for 42 hours at 1000° C.

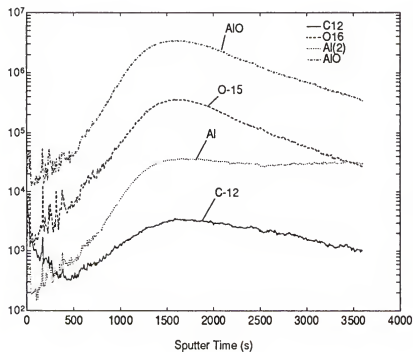


Figure 6-30.
SIMS profile showing C, O, and Al species from a specimen of [110] single-crystal NiAl implanted with 2×10^{17} ^{12}C ions/cm² at 100 keV and subsequently oxidized for 42 hours at 1000° C.

a thinner surface oxide layer than the C implanted (or non-implanted) surfaces. At this point however the utility of SIMS analysis of the oxide layers has reached its limit. The results to this point were sufficiently positive to pursue a brief cyclic oxidation experiment however.

Cyclic Oxidation of Oxygen-Implanted NiAl

Since the specimens used in this investigation were not implanted over their entire surface, thermogravimetric analysis results in data which averages the kinetics of non-implanted and implanted surfaces. The most important problem with oxidation of NiAl is scale adherence under cyclic oxidation however. Therefore a cyclic oxidation experiment was conducted in which a specimen of [211] oriented single crystal NiAl, implanted on one side with 1×10^{18} ^{16}O ions/cm². The sample was eight cycles to 1000° C each of 2 hour duration for a total exposure of 16 hours. The atmosphere in this case was Ar-20% O₂. A Cahn TG-171 TGA was utilized to monitor weight change during the exposure, however since the kinetics of oxidation were not representative of a completely implanted sample, no rate constant was derived from this data. Figure 6-31 shows the raw TGA curve superimposed with the cyclic temperature profile. Figure 6-32 shows the composite TGA curve, where weight changes due to buoyancy effects have been eliminated. Careful examination of these figures shows that some scale spallation did occur during each cooldown cycle. After the conclusion of the experiment it was clear that nearly all of the spallation occurred on the non-implanted surfaces. Figures 6-33 and 6-34 are SEM micrographs from the non-implanted and oxygen-implanted areas of this

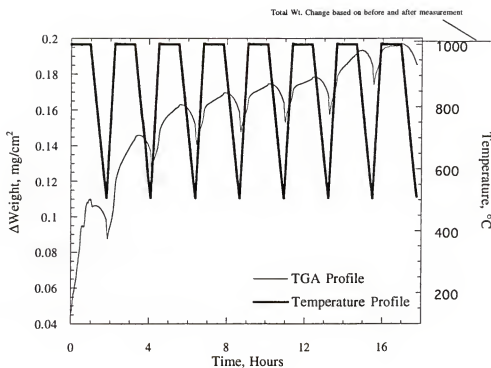


Figure 6-31. TGA profile superimposed with cyclic temperature profile from a specimen of [211] NiAl implanted on most of one side with 1×10^{18} ^{16}O ions/ cm^2 exposed for a eight 2-hour cycles at 1000 $^{\circ}\text{C}$.

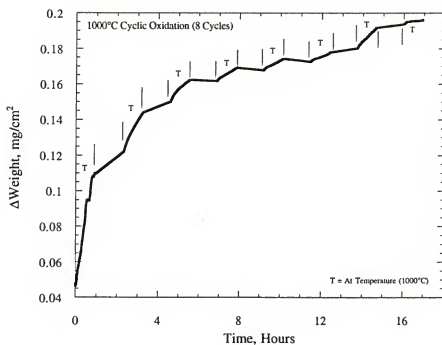


Figure 6-32. TGA profile from a specimen of [211] NiAl implanted on most of one side with 1×10^{18} ^{16}O ions/cm² exposed for a eight 2-hour cycles at 1000° C. This is the same data shown in fig. 6-26, with the weight changes due to temperature effects removed.

specimen. prior to exposure both of these areas had exactly the same surface finish. All of the non-implanted area had the same surface topography, characterized by the whisker morphology characteristic of theta alumina. Almost all of the oxygen implanted surface showed only slightly more surface relief prior to exposure. a few small areas of the implanted surface did spall however. Figure 6-35 shows a micrograph of a spalled area in the implanted surface. Where the implanted surface did spall the typical whisker morphology was again observed. Therefore while this experiment was not an unqualified success, the very limited amount of spallation shows that the implanted surface does result in improved oxidation resistance under cyclic oxidation. Since the implanted layer is very thin it is quite possible that the areas that did fail were damaged prior to exposure.

Summary

In the as-implanted state the oxygen-implanted layer in NiAl consists of a mixture of partially oxidized aluminum and nickel. Upon annealing the implanted layer reorders into a continuous oxide layer with an epitaxial relationship to the substrate. This layer does not however correspond to any of the previously recorded binary alumina structures. There is a reasonable match with the cubic ternary oxide NiAl_2O_4 . The implanted oxide has been shown to be clearly stable at times up to 1 hour under oxidizing conditions. The implanted layer has been shown to result in improved oxidation resistance at up to 42 hours under isothermal conditions as well as under short-term cyclic oxidation. This proves the principle that implantation of oxygen, at sufficient concentrations to form a continuous oxide layer, can form a protective layer that reduces the subsequent rate of high temperature oxidation.



Figure 6-33. SEM micrograph of the non-implanted area of the specimen of [211] NiAl implanted on most of one side with 1×10^{18} ^{16}O ions/cm² exposed for a eight 2-hour cycles at 1000° C. This topography is characteristic of all of the non-implanted surface and indicates the formation of theta alumina.



Figure 6-34. SEM micrograph of the oxygen-implanted area of the specimen of [211] NiAl implanted on most of one side with 1×10^{18} ^{16}O ions/cm² exposed for a eight 2-hour cycles at 1000° C. This topography is characteristic of most of the implanted surface.



Figure 6-35. SEM micrograph of a spalled area of the implanted surface of the specimen of [211] NiAl implanted on most of one side with 1×10^{18} ^{16}O ions/cm² exposed for a eight 2-hour cycles at 1000° C.

CHAPTER 7 SUMMARY AND CONCLUSIONS

Review of Research Objectives

The objective of this research was to determine whether an oxide layer could be formed by ion implantation of oxygen into binary aluminide intermetallic compounds. Once it could be determined that an oxide was formed by implantation, the further objective was to investigate the stability of the implanted layer at high temperature. Finally, if the layer proved to be stable, the final objective was assess its effect on the high temperature oxidation kinetics of the particular material. The overall goal of this research is to prove the principal that by bypassing the initial oxidation stage at high-temperature by preoxidation at room temperature, the resulting kinetics of high temperature oxidation could be significantly improved. Three intermetallic compounds, NiAl, NbAl₃, and TiAl, with well-studied oxidation mechanisms were used. Each of the three exhibits at least one important oxidation problem which might be improved by preoxidation at room temperature. All of the major objectives were met with some success in each of the compounds studied. These are each reviewed in detail below.

Oxygen-Implanted NbAl₃

Using Auger spectroscopy to determine the oxidation state of the Al in the implanted layer, it was shown that an oxide consisting primarily of alumina was formed in

the as-implanted NbAl_3 . The structure of this layer is apparently not a regular crystal as no diffraction pattern was observed beyond that due to the substrate. After annealing and oxidation treatments, diffraction patterns attributable to alpha alumina and NbAl_3 were observed, which suggests that the implanted layer recrystallizes into equilibrium phases at high temperature. SIMS analysis of the scale composition and thickness on both non-implanted and oxygen implanted surfaces showed that under all conditions tested, the implanted layer results in a decrease in the subsequent oxygen penetration of the surface during high-temperature oxidation. This proves the principal that improved oxidation resistance can be achieved by pre-oxidizing at room temperature using ion implantation.

The "pestring" phenomenon of specimen disintegration at intermediate temperatures and low oxygen activities was also studied using oxygen-implanted NbAl_3 . A significant improvement in the resistance to pestring was observed in all of the implanted specimens. It was shown that this improvement was associated with significantly reduced oxygen penetration into the substrate material, due to the presence of the oxygen implanted barrier layer. This further shows that the mechanism of pest is dependent on oxygen dissolution in the substrate, rather than simply penetration down grain boundaries. Furthermore the pestring mechanism of Topylgo and Grabke¹² which proposes that the controlling mechanism of pestring is phase transformation from NbAl_3 to Nb_2Al due to loss of Al along grain boundaries, is not supported by these results.

Oxygen Implanted TiAl

In the as-implanted state, Auger and SIMS data show that an oxide layer is formed in the implanted region of the TiAl specimens. Auger spectra show that the structure of the implanted layer contains a mixture of partially oxidized titanium and aluminum. Of the two substrate elements, the aluminum appears to have captured the majority of the oxygen however the energy shift in the Al LVV peak which is observed is consistent with formation of Al_2O_3 , while the changes which occur in the Ti MVV spectra are most consistent with Ti metal and a minor fraction of TiO. X-ray diffraction does not reveal any peaks attributable to the as-implanted layer therefore the structure of this layer is taken to be highly disordered and not consistent with any particular crystal structure.

After short oxidation exposures at high temperature the oxygen-implanted layer resulted in slightly thicker oxide layers than on the non-implanted areas of the same specimens. Comparison with specimens implanted with an identical dose of an inert ion, ^{20}Ne , showed that the radiation damage caused by the implantation results in accelerated formation of titanium oxide on the surface of the material. Using SIMS the implanted ^{18}O was observed to begin to dissolve into the substrate material after very short exposures at 1000°C .

The conclusion drawn from these results is that although it is possible to form aluminum oxide at room temperature by oxygen implantation of TiAl, the damage caused by the implantation and the high oxygen solubility of the substrate makes the implanted layer unstable at high temperature and results in more rapid formation of oxide phases which do not result in protective oxidation kinetics. The fundamental problem of forming

a slow-growing protective oxide layer on an material containing two elements whose oxides have similar stabilities is not amenable to improvement using oxygen implantation. This conclusion applies to any alloys fitting the above description, particularly TiAl.

Oxygen-Implanted NiAl

In the as-implanted state the oxygen implanted layer on single crystal NiAl was shown to consist of metallic Ni and oxidized Al. The energy peak shift observed in the Al LVV Auger spectra were not consistent with formation of Al_2O_3 . Therefore the as-implanted layer is best described as a supersaturated solution of oxygen in NiAl with containing a mixture of metallic and unsaturated oxide bonds.

After a short annealing treatment at 1000°C , the implanted layer recrystallized into an oxide with an epitaxial relationship to the substrate. X-ray diffraction revealed the presence of a single diffraction peak due to the recrystallized implanted layer. The best match for this peak appears to be NiAl_2O_4 , which is also a reasonable candidate for epitaxial growth on NiAl. Longer term annealing experiments showed that the implanted layer is stable for up to one hour without showing any discernible degradation. Auger depth profiling of annealed specimens showed that the implanted layer consists of a continuous layer of Al_2O_3 containing dissolved Ni. The Ni is observed to be rejected from the implanted layer into the matrix on either side.

Oxidation of oxygen implanted NiAl specimens showed significant improvements in oxidation resistance. Under both isothermal and cyclic exposure the implanted layer resulted in thinner scales with clearly improved resistance to spallation. The presence of

the implanted layer suppresses the formation of the transient oxides associated with the initial oxidation of NiAl. During oxidation the structure of the implanted layer is stable, maintaining the same well defined interfaces. The structure incorporates oxygen from the ambient but retards the transport of oxygen into the substrate.

Taken together all of the initial objectives were satisfied in the oxygen implanted NiAl. The implanted layer was shown to result in a stable, continuous structure unique to the implantation process, The presence of this structure bypassed the formation of transient oxides and resulted in a reduced rate of subsequent scale growth. Further research into this system is clearly warranted. Likely improvements to the implanted layer could be achieved by several routes; Use of a target containing amounts Zr, which has been shown to improve the spallation resistance of oxide scales on NiAl, modified implantation parameters using a range of accelerating energies to obtain a thicker implanted layer which is continuous from the surface down to a micrometer into the surface, or exposure of the implanted specimens at higher temperatures where transient oxide formation occurs more rapidly, to name just a few.

REFERENCES

1. ASM Handbook Vol. 3 Alloy Phase Diagrams, H. Baker, ed., ASM (1992).
2. Joint Committee on Powder Diffraction Standards, JCPDS card # 13-146, JCPDS-ICDD, Swarthmore, Pa., (1988).
3. R.C. Svedberg, "Oxides Associated With the Improved Air Oxidation Performance of Some Niobium intermetallics and Alloys", Properties of High Temperature Alloys, Z.A. Foroulis and F.S. Petit, eds. The Electrochemical Society, Pennington, N.J. (1976), 331-362.
4. R.A. Perkins, K.T. Chiang, and G.H. Meier, Scripta Metallurgica et Materialia, 22 (1988), 419-24.
5. M.P. Brady, The Role of Microstructure During Oxidation in the Nb-Ti-Al System, Ph.D. Dissertation, University of Florida (1993).
6. M.G. Hebsur, J.R. Stephens, J.L. Smialek, C.A. Barrett, and D.S. Fox, "Influence of Alloying Elements on the Oxidation Behavior of NbAl", in Oxidation of High Temperature Intermetallics, T. Grobstein and J. Doychak eds. TMS, Warrendale Pa. (1989).
7. J. Doychak and M.G. Hebsur, Oxidation of Metals, 36 1/2 (1991), 113-41.
8. E.A. Aitken, in Intermetallic Compounds, J.H. Westbrook, ed., Wiley, New York, (1967).
9. M. Steinhorst, and H.J. Grabke, Materials Science and Engineering, A120 (1989), 55-9.
10. H.J. Grabke, M. Steinhorst, M. Brumm, and D. Wiemer, Oxidation of Metals, 35 3/4 (1991), 199-223.
11. V.K. Tolpygo and H.J. Grabke, Scripta Met., 28 (1993) 747-52.
12. G. Welsch and A.I. Kahveci, "Oxidation Behavior of Titanium Aluminide Alloys", in Oxidation of High Temperature Intermetallics, T. Grobstein and J. Doychak eds. TMS, Warrendale Pa. (1989).

13. G.H. Meier, D. Appalonia, R.A. Perkins, and K.T. Chiang, "Oxidation of Ti Base Alloys", in Oxidation of High Temperature Intermetallics, T. Grobstein and J. Doychak eds. TMS, Warrendale Pa. (1989).
14. S. Becker, A. Rahmel, M. Schorr, and M. Schutze, Oxidation of Metals, 38, 5/6, (1992) 425-464.
15. S. Becker, M. Schutze, and A. Rahmel, Oxidation of Metals, 38, 1/2, (1992) 93-106.
16. T. Shimizu, T. Iikubo, and S. Isobe, Materials Science and Engineering, A153, (1992) 602-7.
17. R.W. Beye and R. Gronsky, to be published in Scripta Metallurgica. et Materialia., (1994).
18. S. Taniguchi, T. Shibata, and A. Murakami, Oxidation of Metals., 41, 1/2, (1994).
19. J.H. Westbrook and D.L. Wood, Journal of Nuclear Materials, 12(2), (1964) 208-15.
20. J. Doychak, J.L. Smialek, and C.A. Barrett, "The Oxidation of Ni-Rich NiAl Intermetallics", in Oxidation of High Temperature Intermetallics, T. Grobstein and J. Doychak, eds., TMS, Warrendale, Pa., (1988) 41-55.
21. J. Doychak and M. Ruhle, Oxidation of Metals, 31, 5/6, (1989) 431-53.
22. G. C. Rybicki and J. L. Smialek, Oxidation of Metals, 31, 3/4, (1989) 275-304.
23. E.W.A. Young and J.H.W. de Wit, Oxidation of Metals, 26, 5/6, (1986) 351-61.
24. B.A. Pint, J.R. Martin, and L.W. Hobbs, Oxidation of Metals, 39, 3/4, (1993) 167-95.
25. R. Prescott, D.F. Mitchell, and M.J. Graham, Corrosion Science, 50/1, (1994) 62-71.
26. J. A. Nesbitt, Journal of the Electrochemical Society, 136/5, (May 1989) 1518-27.
27. J.A. Nesbitt and E.J. Vinarcik, "Predicting the Oxidative Lifetime of β NiAl-Zr Alloys", in Damage and Oxidation Protection in High Temperature Intermetallics, G.K. Haritos and O.O. Ochoa, eds., ASME, book No. H0692A, (1991) 9-22.

28. J.A. Nesbitt and C.A. Barrett, "Predicting the Oxidation Limited Lifetime of β NiAl", in Structural Intermetallics, R. Darolia et al. eds. TMS, Warrendale, Pa. (1993) 601-9.
29. C. A. Barrett, Oxidation of Metals, 30 5/6, (1988) 361-90.
30. B.A. Pint and L.W. Hobbs, Oxidation of Metals, 41, 2/4, (1994) 203-31.
31. J. Doychak, J.L. Smialek, and T.E. Mitchell, Metallurgical Transactions A, 20A, (1989) 499-518.
32. D.M. Follstaedt, Nuclear Instruments and Methods in Physics Research, B7/8, (1985) 11-19.
33. I. H. Wilson, Nuclear Instruments and Methods in Physics Research, B1, (1984) 331-43.
34. J.G. Perkins and L.E. Collins, Thin Solid Films, 5, (1970) R59.
35. J.G. Perkins, Thin Solid Films, 9, (1972) 257-72.
36. P.T. Stroud, H. M. Lindsay, and J.G. Perkins, Vacuum, 23/4, (1972) 125-30.
37. S. Chereckddjian and I.H. Wilson, Nuclear Instruments and Methods in Physics Research, B1, (1984) 258-64.
38. A.D. Yadav and S.M. Bhatia, Thin Solid Films, 163, (1988) 317-22.
39. R.G. Musket, D.W. Brown, H.C. Hayden, Nuclear Instruments and Methods in Physics Research, B7/8, (1985) 31-7.
40. R.G. Musket, D.W. Brown, and R.F. Pinizzotto, Applied Physics Letters, 49, (1986) 379.
41. S.M. Myers and D.M. Follstaedt, Journal of Applied Physics, 63(6), (1988) 1942-50.
42. R.J. Bourcier, S.M. Myers, and D.H. Polonis, Nuclear Instruments and Methods in Physics Research, B44, (1990) 278-88.
43. D.M. Follstaedt, S.M. Myers, and R.J. Bourcier, Nuclear Instruments and Methods in Physics Research, B59/60, (1991) 909-13.
44. S. Ohira and M. Iwaki, Materials Science and Engineering, A116, (1989) 153-60.

45. S. Ohira and M. Iwaki, Nuclear Instruments and Methods in Physics Research, B46, (1990) 413-16.
46. S. Ohira and M. Iwaki, Nuclear Instruments and Methods in Physics Research, B19/20, (1987) 162-6.
47. P.T. Stroud, Thin Solid Films, 10, (1972) 205-215.
48. Y. Okabe, M. Iwaki, K. Takahashi, S. Ohira, and B.V Crist, Nuclear Instruments and Methods in Physics Research, B39, (1989) 619-22.
49. Y. Okabe, M. Iwaki, and K. Takahashi, Nuclear Instruments and Methods in Physics Research, B61, (1991) 44-7.
50. J.L. Brimhall, H.E. Kissinger, and L.A. Charlot, Radiation Effects, 77, (1983) 237-93.
51. L.S. Hung, M. Nastasi, J. Gyulai, and J.W. Mayer, Applied Physics Letters, 42(8), (1983) 672-75.
52. J. Delafond, C. Jaouen, J.P. Riviere, and C. Fayoux, Materials Science and Engineering, 69, (1985) 117-21.
53. C. Jaoen, J.P. Riviere, and J. Delafond, Nuclear Instruments and Methods in Physics Research, B59/60, (1991) 406-9.
54. K. Kylesbech Larsen, N. Karpe, J. Bottiger, and R. Bormann, Journal of Materials Research, 7(4), (1992) 861-7.
55. J. Eridon, G.S. Was, and L.Rehn, Journal of Materials Research, 3(4), 626-39, (1988).
56. M. Ahmed and I. Potter, Acta Metallurgica et Materialia, 33(12), (1985) 2221-31.
57. K. Saito and T. Matsushima, Materials Science and Engineering, A115, (1989) 355-9.
58. G.S. Was, Journal of Materials Research, 6(8), (1991) 1615-18.
59. D.A. Boerma and T. Corts, Materials Research Society Symposium Proceedings, volume 235, (1992) 491-96.
60. M. Saqib and D.I. Potter, Materials Science and Engineering, 90, (1987) 81-89.

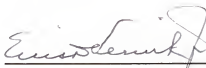
61. K. Pampus, K. Dyrbye, B. Torp, and R. Bormann, Journal of Materials Research, 4(6), (1989) 1385-92,.
62. C.J. McHargue, G.C. Farlow, C.W. White, B.R. Appleton, P. Angelini, and H. Naramoto, Nuclear Instruments and Methods in Physics Research, B10/11, (1985) 569-73.
63. C.W. White, L.A. Boatner, P.S. Sklad, C.J. Mchargue, S.J. Pennycook, M.J. Aziz, G.C. Farlow, and J. Rankin, Materials Research Society Symposium Proceedings, volume 74, (1987) 357-63.
64. S.J. Zinkle, Materials Research Society Symposium Proceedings, volume 128, (1989) 363-8.
65. S.M.M. Ramos, B. Canut, P. Thevenard, M. Bauer, Y. Maheo, Ph. Kapsa, and J.L. Loubet, Journal of Materials Research, 7(1), (1992), 178-84.
66. S.N. Bunker and A.J. Armini, Nuclear Instruments and Methods in Physics Research, B39, (1989), 7-10.
67. L. E. Davis et al. Handbook of Auger Electron Spectroscopy, second edition, Perkin Elmer Corp., Physical Electronics Division, Eden Prairie, Mn., (1979).
68. D. Briggs and M.P. Seah, eds. Practical Surface Analysis by Auger and X-ray Photoelectron Spectroscopy, John Wiley & Sons, New York, N.Y., (1983).
69. R.G. Wilson, F.A. Stevie, and C.W. McGee, Secondary Ion Mass Spectrometry, a Practical Handbook for Depth Profiling and Bulk Impurity Analysis, John Wiley and Sons, (1989).
70. M.P. Seah and W.A. Dench, Surface and Interface Analysis, 1/2, (1979).
71. R.J. Hanrahan Jr., E.D. Verink, S.P. Withrow, and E.O. Ristolainen, "Modification of the Initial Oxidation Kinetics of TiAl, NbAl₃ and 25-25-50 Nb-Ti-Al by Oxygen Ion Implantation" in Processing and Characterization of Advanced Materials IV, V.A. Ravi and T.S. Srivatsan eds., TMS, Warrendale Pa., (1994).
72. R.J. Hanrahan Jr., E.D. Verink, E.O. Ristolainen and S.P. Withrow. "Oxide Formation on TiAl and NbAl₃ Due to High - Dose Ion Implantation of ¹⁸O." in Materials Synthesis and Processing of Materials Using Ion Beams, R.J. Culbertson and K.S. Jones eds. Proceedings of the Materials Research Society Symposium, Vol 316. MRS, (1994).
73. J.S. Solomon and W.L. Baun, Surface Science, 51, (1975) 228-36.

74. S. Nishigaki, Surface Science, 125, (1983) 762-70.
75. T.N. Taylor and M.T. Paffett, Materials Science and Engineering, A153, (1992) 584-90.
76. M.R. Shanabarger, Materials Science and Engineering, A153, (1993) 608-12.
77. Y.T. Peng, P.B. Aswath, and A.R. Koymen, Metallurgical and Materials Transactions A, 25A, (1994) 1041-50.
78. . Joint Committee on Powder Diffraction Standards, JCPDS card # 20-19 (NiAl) JCPDS-ICDD, Swarthmore, Pa., (1988).
79. .Joint Committee on Powder Diffraction Standards, JCPDS card # 10-339 (NiAl₂O₄) JCPDS-ICDD, Swarthmore, Pa., (1988).
80. Joint Committee on Powder Diffraction Standards, JCPDS card # 10-173 (α Alumina), JCPDS-ICDD, Swarthmore, Pa., (1988).

BIOGRAPHICAL SKETCH

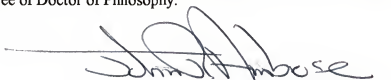
Robert Joseph Hanrahan Jr. was born in Gainesville, Florida, on April 21, 1965. He has attended school within walking distance of the hospital where he was born for his entire academic career. He graduated from Buchholz High School in May, 1982. In August, 1982 he began attending the University of Florida, graduating with a bachelors degree in nuclear engineering in December, 1987. In August, 1988 he began graduate studies in the nuclear engineering program at UF, receiving a masters degree in nuclear engineering in December, 1990. In January, 1991 he officially began studies in the materials science and engineering department at UF. Since 1991 he has been employed on an intermittent basis by Los Alamos National Laboratory as a graduate research assistant. In addition to academic pursuits Mr. Hanrahan pursues several hobbies, chief among them automobile restoration and photography. After completing his long career as a UF student he plans to accept a postdoctoral appointment at LANL. As a long term goal he hopes to have the opportunity to become a Professor.

I certify that I have read this study and that in my opinion it conforms to acceptable standards of scholarly presentation and is fully adequate, in scope and quality, as a dissertation for the degree of Doctor of Philosophy.



Ellis D. Verink Jr., Chairman
Distinguished Service Professor of Materials
Science and Engineering

I certify that I have read this study and that in my opinion it conforms to acceptable standards of scholarly presentation and is fully adequate, in scope and quality, as a dissertation for the degree of Doctor of Philosophy.



John R. Ambrose
Associate Professor of Materials Science and
Engineering

I certify that I have read this study and that in my opinion it conforms to acceptable standards of scholarly presentation and is fully adequate, in scope and quality, as a dissertation for the degree of Doctor of Philosophy.



Samim Anghaie
Professor of Nuclear Sciences and Engineering

I certify that I have read this study and that in my opinion it conforms to acceptable standards of scholarly presentation and is fully adequate, in scope and quality, as a dissertation for the degree of Doctor of Philosophy.



Stanley R. Bates
Associate Engineer of Materials Science and
Engineering

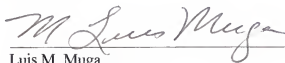
I certify that I have read this study and that in my opinion it conforms to acceptable standards of scholarly presentation and is fully adequate, in scope and quality, as a dissertation for the degree of Doctor of Philosophy.



Robert T. DeHoff

Professor of Materials Science and Engineering

I certify that I have read this study and that in my opinion it conforms to acceptable standards of scholarly presentation and is fully adequate, in scope and quality, as a dissertation for the degree of Doctor of Philosophy.

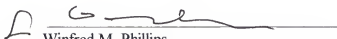


Luis M. Muga

Professor of Chemistry

This dissertation was submitted to the Graduate Faculty of the College of Engineering and to the Graduate School and was accepted as partial fulfillment of the requirements for the degree of Doctor of Philosophy.

December 1994



Winfred M. Phillips

Dean, College of Engineering



Karen A. Holbrook

Dean, Graduate School